Free in-plane vibration analysis of a rectangular plate with an edge V-notch

Xutao Sun[a,*]
[a]The School of Engineering, University of Waikato, Hamilton, 3216, New Zealand
*Corresponding author.
E-mail address: xutao.sun@waikato.ac.nz
ORCID: 0000-0002-2874-7742

Abstract

In-plane vibration affects high-frequency energy transmission and the dynamic response of built-up plate structures. Edge V-notches, arising from cutouts, machining, or accidental damage, are common in plates. Although such notches can substantially alter plate modal characteristics, the free in-plane vibration of V-notched plates remains unstudied. This paper develops an enriched Ritz method for the free in-plane vibration of a rectangular plate with an edge V-notch. The two coupled in-plane displacement components are approximated by a global trigonometric-polynomial basis augmented with symmetric and antisymmetric corner functions re-derived from Williams's asymptotic solution for a traction-free angular corner in extension. Essential boundary conditions are enforced strongly through separate boundary multipliers for each displacement component, while the energy integrals are evaluated over the physical notched domain using high-order triangular quadrature. Convergence studies show that the method reproduces published intact plate solutions with monotonic upper-bound convergence to at least four significant figures. For V-notched plates, the calculated frequency parameters converge from above to at least three significant figures and agree closely with finite element results. Corner enrichment becomes increasingly important as the notch sharpens. The leading roots between 0 and 1 provide large corrections to frequencies, with additional higher-order roots giving diminishing improvement. Benchmark frequency parameters and mode shapes are presented for a free square plate with a centrally located vertical V-notch, showing that notch depth is the dominant geometric parameter and notch angle has a secondary effect.

Keywords: In-plane vibration; Rectangular plate; V-notch; Ritz method; Stress singularity; Natural frequency; Mode shape

1 Introduction

Rectangular plates are fundamental structural components in engineering applications ranging from aerospace panels and ship hulls to civil infrastructure. A vibrating flat plate can exhibit three types of wave motion: transverse bending, longitudinal, and shear. Of these, the latter two together constitute the in-plane vibrations, which, although they typically occur at higher frequencies than the fundamental transverse modes, are of considerable importance. It has been shown that in-plane vibrations play a major role in the transmission of high-frequency vibration energy through built-up structures [1-3]. In-plane vibrations are directly coupled to out-of-plane motion whenever plates are connected at an angle, meaning that even within a low-frequency analysis, the in-plane stiffness can meaningfully influence the response at structural junctions [4]. In-plane vibrations also have direct implications for noise radiation into the surrounding environment [5]. Accurate prediction of the in-plane natural frequencies and mode shapes is therefore of both theoretical and practical importance.

Sharp edge cutouts such as V-notches are introduced to rectangular plates for various purposes, for example, to provide clearance for pipes, cables, or intersecting members, to allow access to welds, joints, or adjacent components, and to provide locating features during assembly. A V-notch may also result from machining operations and punched or laser cut profiles. In addition, a V-notch can represent edge deterioration or accidental damage in thin-walled structural members, machine casings, aerospace and marine panels, etc. Because the notch modifies the membrane load path and introduces a strong stress concentration at its vertex, it can significantly influence the in-plane natural frequencies and mode shapes of the plate. However, the free vibration of rectangular plates with edge V-notches has received little attention, especially the free in-plane vibration, where it is difficult to derive solutions from the governing equations involving two independent displacement components, and incorporating the asymptotic displacement field near the notch vertex poses an additional challenge.

The free in-plane vibration of rectangular plates has received relatively less research attention compared with the well-developed body of literature on transverse vibration. Kobayashi *et al.* [6] appear to be among the first to study in-plane vibration of rectangular plates via the Ritz method, computing natural frequencies for point-supported configurations using power series expansions. Bardell *et al.* [7] subsequently applied the Ritz method with hierarchical K-orthogonal polynomial admissible functions to obtain benchmark results for free, clamped, and simply supported rectangular plates. Wang and Wereley [8] investigated in-plane vibration using the Kantorovich-Krylov variational method. A series of analytical-type solutions for plates with classical boundary conditions were obtained by Gorman [5, 9, 10] via the superposition method, providing benchmark results for a range of aspect ratios. Exact closed-form solutions for all combinations of classical boundary conditions (with at least two opposite plate edges having either type of the simply-supported conditions) were subsequently established using direct separation of variables [11, 12]. For plates with elastic boundary restraints, exact methods become inapplicable, and the Ritz method offers a natural alternative. An early treatment of elastically restrained edges was given by Gutierrez and Laura [13]. Dozio [14] developed a Ritz formulation with trigonometric admissible functions and an artificial edge-spring technique to enforce arbitrary boundary conditions variationally, demonstrating rapid convergence and good agreement with exact solutions for intact plates. Alternatively, Du *et al.* [4] proposed an improved Fourier series method which expresses the in-plane displacements as the superposition of a double Fourier cosine series and four supplementary polynomial-cosine terms to eliminate derivative discontinuities at the edges, and demonstrated highly accurate solutions for rectangular plates with general elastic edge restraints. Further extensions of free in-plane vibration include orthotropic and laminated composite plates [15], non-uniform elastic supports [16], composite plates of arbitrary polygonal shape [17], and plates with curved edges [18, 19].

The analytical treatment of transverse free vibration in plates with re-entrant corners has developed extensively through the systematic integration of singular field representations into global numerical frameworks. Early contributions established the asymptotic expression for stress singularities near geometric discontinuities: Williams [20, 21] showed that, for plates in extension and bending, the displacement field near a corner or crack tip takes a characteristic singular form whose order is determined by an eigenvalue problem depending on the opening angle and boundary conditions. Building on this foundation, Leissa *et al.* [22] and McGee *et al.* [23, 24] established that the standard Ritz method, when augmented with Williams-type corner functions that exactly represent the bending moment and stress singularities at a notch vertex or crack tip, provides highly accurate frequency parameters for circular plates and sectorial configurations. This hybrid methodology was later extended by Kim and Jung [25] and Huang *et al.* [26] to investigate the transverse vibration of rhombic plates and rectangular plates, respectively, demonstrating that the inclusion of these corner functions substantially accelerates numerical convergence compared to admissible function sets using complete algebraic polynomials or algebraic-trigonometric polynomials alone. Advancing toward three-dimensional vibrations, McGee and Kim [27] employed the variational Ritz procedure rooted in 3D elasticity theory for thick circular plates and cylinders. Their methodology also utilizes hybrid admissible functions that contain specialized 3D edge functions. These edge functions are derived to explicitly represent the tri-axial stress singularities occurring along the re-entrant terminus edge of V-notches or sharp radial cracks. More recent investigations have evaluated piezoceramic circular plates containing V-notches using the Ritz method, with frequencies and mode shapes validated by electronic speckle pattern interferometry [28, 29]. Yang *et al.* [30] investigated the transverse vibration of moderately thick V-notched Mindlin circular plates using the Ritz method, considering free or clamped radial edges of the V-notch. Despite these comprehensive studies on out-of-plane and three-dimensional vibration, the specific problem of free in-plane vibration in plates with edge V-notches remains unaddressed. The present work fills this gap.

The present study addresses this problem through an enriched Ritz method specifically developed for the coupled in-plane displacement field of a rectangular plate containing an edge V-notch. The two coupled displacement components are represented by a global trigonometric-polynomial basis augmented with symmetric and antisymmetric corner functions derived from Williams's asymptotic solution for a traction-free angular corner in extension. Unlike prior applications of Williams-type enrichment to transverse plate vibration, the corner functions here are re-derived for the coupled in-plane displacement field. Classical boundary conditions are imposed strongly through separate boundary multipliers for the two in-plane displacement components, while the energy integrals are evaluated over the physical notched domain using high-order triangular quadrature. The formulation is validated through extensive convergence studies and new benchmark frequency parameters and mode shapes for a free square plate with a vertical V-notch are presented.

2 Formulation

Consider a thin isotropic rectangular plate occupying $0 \le x \le a$, $0 \le y \le b$ (as shown in Fig. 1) with thickness h, density ρ, Young's modulus E, and Poisson's ratio ν. A V-notch opens from the right edge with vertex angle γ, vertex location c, notch depth d, and is symmetric about its bisector. A local polar coordinate system (r, θ) is centred at the notch vertex $\mathrm{O}(x_0, y_0) = (a - d, c)$ and $\theta = 0$ is aligned with the negative x-direction. The two traction-free notch faces are located at $\theta = \pm\kappa$ with $\kappa = \pi - \frac{\gamma}{2}$, and the material angle around the notch vertex is $\varpi = 2\kappa = 2\pi - \gamma$. The boundary conditions for a rectangular plate are specified by four letters, which refer to the edges $x = 0$, $y = 0$, $x = a$, and $y = b$, respectively. Letters C and F denote clamped and free boundary conditions, respectively. As noted by Gorman [5], two distinct forms of simply supported boundary conditions can arise in the in-plane vibration analysis of rectangular plates. These are denoted here as S_1 and S_2. An S_1-type edge corresponds to zero displacement parallel to the edge and zero normal stress perpendicular to the edge, whereas the S_2-type edge corresponds to zero displacement normal to the edge and zero shear stress along the edge.

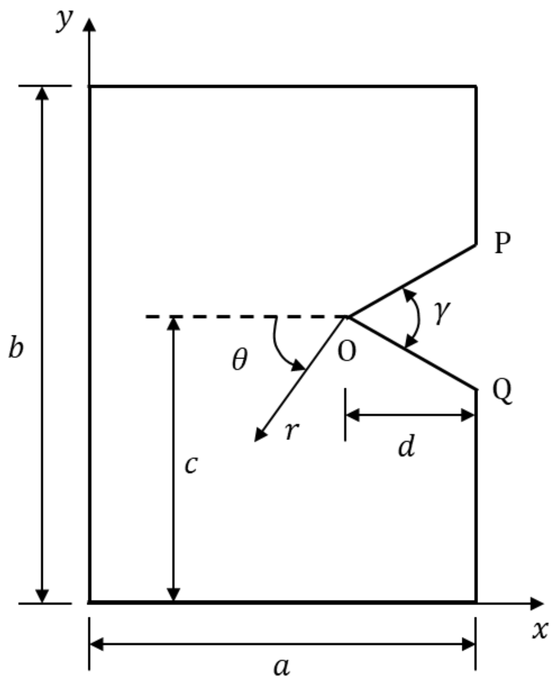

Fig. 1. Dimensions and coordinates for a V-notched plate.

2.1 In-plane energy formulation

For in-plane vibration, the displacement of the plate in the x and y directions are $u = u(x, y, t)$ and $v = v(x, y, t)$, respectively. Let Ω denote the mid-plane domain of the notched plate. The membrane strain energy is

$$\mathcal{U} = \frac{1}{2}\iint_{\Omega} \left[A_{11}\left(\frac{\partial u}{\partial x}\right)^2 + 2A_{12}\frac{\partial u}{\partial x}\frac{\partial v}{\partial y} + A_{22}\left(\frac{\partial v}{\partial y}\right)^2 + A_{66}\left(\frac{\partial u}{\partial y} + \frac{\partial v}{\partial x}\right)^2\right] d\Omega \tag{1}$$

where $A_{11} = A_{22} = Eh/(1-\nu^2)$, $A_{12} = \nu A_{11}$, and $A_{66} = Eh/[2(1+\nu)]$. The kinetic energy of the plate is given by

$$\mathcal{T} = \frac{1}{2}\rho h \iint_{\Omega} \left[\left(\frac{\partial u}{\partial t}\right)^2 + \left(\frac{\partial v}{\partial t}\right)^2\right] d\Omega \tag{2}$$

Introducing the non-dimensional coordinates $\xi = \frac{2x}{a} - 1, \eta = \frac{2y}{b} - 1$, and considering a harmonic motion with frequency ω, i.e.

$$\begin{cases} u(\xi, \eta, t) = U(\xi, \eta) e^{j\omega t} = U e^{j\omega t} \\ v(\xi, \eta, t) = V(\xi, \eta) e^{j\omega t} = V e^{j\omega t} \end{cases} \tag{3}$$

the maximum strain energy $\mathcal{U}_{max}$ and the maximum kinetic energy $\mathcal{T}_{max}$ can be written as

$$\mathcal{U}_{\max} = \frac{1}{2} \iint_{\Omega} \left[A_{11} \frac{b}{a} \left(\frac{\partial U}{\partial \xi} \right)^2 + A_{22} \frac{a}{b} \left(\frac{\partial V}{\partial \eta} \right)^2 + 2A_{12} \frac{\partial U}{\partial \xi} \frac{\partial V}{\partial \eta} + A_{66} \frac{a}{b} \left(\frac{\partial U}{\partial \eta} \right)^2 + A_{66} \frac{b}{a} \left(\frac{\partial V}{\partial \xi} \right)^2 + 2A_{66} \frac{\partial U}{\partial \eta} \frac{\partial V}{\partial \xi} \right] d\xi d\eta \tag{4}$$

and

$$\mathcal{T}_{max} = \frac{1}{2} \frac{\rho h a b}{4} \omega^2 \iint_{\Omega} (U^2 + V^2) \, d\xi d\eta \tag{5}$$

Equations (4)-(5) are evaluated only over the physical notched domain. The triangular notch region is excluded from the domain integration.

2.2 Displacement field of the notched plate

In the Ritz method, the displacement field is approximated by admissible trial functions containing unknown coefficients. For the present V-notched plate, the admissible displacement field is constructed from a regular component and a Williams-type corner-enriched component. Since the outer rectangular edges are treated using classical boundary conditions, the essential boundary conditions are imposed strongly through boundary multipliers. For a generic dimensionless coordinate $z \in [-1,1]$, define

$$\widetilde{H}^{\alpha\beta}(z) = \left(\frac{1+z}{2} \right)^{\delta_\alpha} \left(\frac{1-z}{2} \right)^{\delta_\beta}, \qquad \delta_0 = 1, \quad \delta_* = 0 \tag{6}$$

where the superscript $\alpha\beta$ indicates the essential displacement condition at the two ends of the interval. The first symbol corresponds to $z = -1$, and the second symbol corresponds to $z = 1$. The symbol 0 denotes a prescribed zero displacement, whereas $*$ denotes an unconstrained displacement. The normalised boundary multiplier is

$$H^{\alpha\beta}(z) = \frac{\widetilde{H}^{\alpha\beta}(z)}{\max\limits_{-1 \le z \le 1} \left| \widetilde{H}^{\alpha\beta}(z) \right|} \tag{7}$$

This gives the following boundary multipliers for possible pairs of boundaries,

$$\begin{cases} H^{00}(z) = 1 - z^2 \\ H^{0*}(z) = \dfrac{1+z}{2} \\ H^{*0}(z) = \dfrac{1-z}{2} \\ H^{**}(z) = 1 \end{cases} \tag{8}$$

The base functions are chosen as a trigonometric-polynomial sequence,

$$\begin{cases} \chi_1(z) = 1 \\ \chi_2(z) = z \\ \chi_{2k+1}(z) = \cos(k\pi z), \quad k = 1,2,\dots \\ \chi_{2k+2}(z) = \sin(k\pi z), \quad k = 1,2,\dots \end{cases} \tag{9}$$

where the constant and linear terms are included to represent the rigid-body translation and rotation when permitted by the boundary conditions; the sine and cosine terms provide a rich approximation space for both even and odd displacement variations.

Let the four plate edges be ordered as

$$L{:}\,\xi = -1, \qquad B{:}\,\eta = -1, \qquad R{:}\,\xi = 1, \qquad T{:}\,\eta = 1 \tag{10}$$

For the U-component, define

$$\begin{aligned} \alpha_\xi^U &= \begin{cases} 0, & L = C \text{ or } S_2, \\ *, & L = F \text{ or } S_1, \end{cases} \quad \beta_\xi^U = \begin{cases} 0, & R = C \text{ or } S_2, \\ *, & R = F \text{ or } S_1, \end{cases} \\ \alpha_\eta^U &= \begin{cases} 0, & B = C \text{ or } S_1, \\ *, & B = F \text{ or } S_2, \end{cases} \quad \beta_\eta^U = \begin{cases} 0, & T = C \text{ or } S_1, \\ *, & T = F \text{ or } S_2. \end{cases} \end{aligned} \tag{11}$$

For the V-component, define

$$\begin{aligned} \alpha_\xi^V &= \begin{cases} 0, & L = C \text{ or } S_1, \\ *, & L = F \text{ or } S_2, \end{cases} \quad \beta_\xi^V = \begin{cases} 0, & R = C \text{ or } S_1, \\ *, & R = F \text{ or } S_2, \end{cases} \\ \alpha_\eta^V &= \begin{cases} 0, & B = C \text{ or } S_2, \\ *, & B = F \text{ or } S_1, \end{cases} \quad \beta_\eta^V = \begin{cases} 0, & T = C \text{ or } S_2, \\ *, & T = F \text{ or } S_1. \end{cases} \end{aligned} \tag{12}$$

This component-wise definition reflects the fact that U is normal to vertical edges and tangential to horizontal edges, whereas V is tangential to vertical edges and normal to horizontal edges.

The two-dimensional boundary multipliers for the U- and V-components are then defined as

$$\begin{cases} D_U(\xi,\eta) = H^{\alpha_\xi^U \beta_\xi^U}(\xi) H^{\alpha_\eta^U \beta_\eta^U}(\eta) \\ D_V(\xi,\eta) = H^{\alpha_\xi^V \beta_\xi^V}(\xi) H^{\alpha_\eta^V \beta_\eta^V}(\eta) \end{cases} \tag{13}$$

The unmodulated regular displacement components are approximated by

$$\begin{cases} \hat{U}_p(\xi,\eta) = \sum_{m=1}^{M} \sum_{n=1}^{N} A_{mn}\, \chi_m(\xi) \chi_n(\eta) \\ \hat{V}_p(\xi,\eta) = \sum_{m=1}^{M} \sum_{n=1}^{N} B_{mn}\, \chi_m(\xi) \chi_n(\eta) \end{cases} \tag{14}$$

where A_{mn} and B_{mn} are unknown Ritz coefficients.

Following the solution procedure given in Williams [20] for the in-plane extension problem, which shows that stress singularities occur at the tip of a V-notch when $\gamma < 180^\circ$, one can derive the corner functions for a V-notch with two free edges as follows (the detailed derivation of the corner functions is given in Section 1 of the supplementary material)

$$U_{r,n}^{(A)} = \frac{r^{\lambda_n^{(A)}}}{2\mu} \left\{ -(\lambda_n^{(A)} + 1)\sin[(\lambda_n^{(A)} - 1)\kappa]\sin[(\lambda_n^{(A)} + 1)\theta] + (\lambda_n^{(A)} + 1 - \frac{4\lambda_n^{(A)}}{1+\nu})\sin[(\lambda_n^{(A)} + 1)\kappa]\sin[(\lambda_n^{(A)} - 1)\theta] \right\} \tag{15}$$

$$U_{\theta,n}^{(A)} = \frac{r^{\lambda_n^{(A)}}}{2\mu} \left\{ -(\lambda_n^{(A)} + 1)\sin[(\lambda_n^{(A)} - 1)\kappa]\cos[(\lambda_n^{(A)} + 1)\theta] + (\lambda_n^{(A)} - 1 + \frac{4\lambda_n^{(A)}}{1+\nu})\sin[(\lambda_n^{(A)} + 1)\kappa]\cos[(\lambda_n^{(A)} - 1)\theta] \right\} \tag{16}$$

$$U_{r,n}^{(S)} = \frac{r^{\lambda_n^{(S)}}}{2\mu} \left\{ -(\lambda_n^{(S)} + 1)\cos[(\lambda_n^{(S)} - 1)\kappa]\cos[(\lambda_n^{(S)} + 1)\theta] + (\lambda_n^{(S)} + 1 - \frac{4\lambda_n^{(S)}}{1+\nu})\cos[(\lambda_n^{(S)} + 1)\kappa]\cos[(\lambda_n^{(S)} - 1)\theta] \right\} \tag{17}$$

$$U_{\theta,n}^{(S)} = \frac{r^{\lambda_n^{(S)}}}{2\mu}\left\{(\lambda_n^{(S)}+1)\cos[(\lambda_n^{(S)}-1)\kappa]\sin[(\lambda_n^{(S)}+1)\theta] - (\lambda_n^{(S)}-1+\frac{4\lambda_n^{(S)}}{1+\nu})\cos[(\lambda_n^{(S)}+1)\kappa]\sin[(\lambda_n^{(S)}-1)\theta]\right\} \tag{18}$$

where $U_{r,n}$ and $U_{\theta,n}$ denote the radial and circumferential displacements, respectively; the superscripts (A) and (S) indicate antisymmetric and symmetric, respectively; μ is the shear modulus; and $\lambda_n^{(A)}$ and $\lambda_n^{(S)}$, respectively, are roots of the following equations

$$\sin\left(\lambda_n^{(A)}\varpi\right) = \lambda_n^{(A)}\sin\varpi \tag{19}$$

$$\sin\left(\lambda_n^{(S)}\varpi\right) = -\lambda_n^{(S)}\sin\varpi \tag{20}$$

Roots satisfying $0 < \lambda < 1$ are especially important because the corresponding stresses behave as $r^{\lambda-1}$ and are therefore singular at the notch vertex. For a prescribed notch opening angle $0 < \gamma < \pi$, Eqs. (19)-(20) are solved numerically to obtain the admissible Williams eigenvalues. Since $\varpi = 2\pi - \gamma$ and $\sin\varpi = -\sin\gamma$, the boundedness of the sine function implies that any positive real root must satisfy $0 < \lambda \leq 1/\sin\gamma$. Thus, for a fixed non-zero V-notch opening angle, only a finite number of positive real roots exists. In the numerical implementation, the positive roots of Eqs. (19)-(20) are identified on this finite interval using a bracketing procedure and MATLAB's *fzero* function. The root $\lambda = 1$, which corresponds to a bounded-stress term, is excluded from the retained singular enrichment as mentioned in Section 1 of the supplementary material.

The Ritz displacement field is expressed in terms of the Cartesian displacement components U and V. Since the local radial direction is measured from the negative x-axis, the polar displacement components are transformed into Cartesian components as

$$\begin{cases} U_{x,n}^{(q)} = -U_{r,n}^{(q)}\cos\theta + U_{\theta,n}^{(q)}\sin\theta \\ U_{y,n}^{(q)} = U_{r,n}^{(q)}\sin\theta + U_{\theta,n}^{(q)}\cos\theta \end{cases} \tag{21}$$

where $q = A, S$. The unmodulated corner-enriched displacement components are then written as

$$\begin{cases} \hat{U}_c(r,\theta) = \sum_{n=1}^{N_A} C_n^{(A)}\, U_{x,n}^{(A)}(r,\theta) + \sum_{n=1}^{N_S} C_n^{(S)}\, U_{x,n}^{(S)}(r,\theta) \\ \hat{V}_c(r,\theta) = \sum_{n=1}^{N_A} C_n^{(A)}\, U_{y,n}^{(A)}(r,\theta) + \sum_{n=1}^{N_S} C_n^{(S)}\, U_{y,n}^{(S)}(r,\theta) \end{cases} \tag{22}$$

where $C_n^{(A)}$ and $C_n^{(S)}$ are additional Ritz coefficients; N_A and N_S denote the numbers of retained antisymmetric and symmetric Williams roots, respectively, and are limited by the number of available positive roots of Eqs. (19)-(20) for the specified notch angle. Each Williams corner function represents one local displacement pattern near the notch vertex. After transformation from polar to Cartesian coordinates, this single local pattern has two components, $U_{x,n}^{(q)}$ and $U_{y,n}^{(q)}$. These two components should therefore share the same Ritz coefficient so that the relative x- and y-displacement amplitudes given by the Williams solution are retained.

The complete admissible displacement field is finally expressed as

$$\begin{cases} U(\xi,\eta) = D_U(\xi,\eta)\left[\widehat{U}_p(\xi,\eta) + \widehat{U}_c(r,\theta)\right] \\ V(\xi,\eta) = D_V(\xi,\eta)\left[\widehat{V}_p(\xi,\eta) + \widehat{V}_c(r,\theta)\right] \end{cases} \tag{23}$$

Equivalently,

$$\begin{cases} U(\xi,\eta) = D_U(\xi,\eta)\left[\sum_{m=1}^{M}\sum_{n=1}^{N} A_{mn}\,\chi_m(\xi)\chi_n(\eta) + \sum_{n=1}^{N_A} C_n^{(A)}\,U_{x,n}^{(A)}(r,\theta) + \sum_{n=1}^{N_S} C_n^{(S)}\,U_{x,n}^{(S)}(r,\theta)\right] \\ V(\xi,\eta) = D_V(\xi,\eta)\left[\sum_{m=1}^{M}\sum_{n=1}^{N} B_{mn}\,\chi_m(\xi)\chi_n(\eta) + \sum_{n=1}^{N_A} C_n^{(A)}\,U_{y,n}^{(A)}(r,\theta) + \sum_{n=1}^{N_S} C_n^{(S)}\,U_{y,n}^{(S)}(r,\theta)\right] \end{cases} \tag{24}$$

It is worth noting that the functions $\widehat{U}_c$ and $\widehat{V}_c$ reproduce the local asymptotic displacement fields associated with a traction-free V-notch. After multiplication by the boundary multipliers D_U and D_V, they are used as admissible enrichment functions in the global Ritz approximation. Since the notch vertex is located away from the outer rectangular boundaries, D_U and D_V are smooth and non-zero near the vertex. Thus, the multiplication preserves the leading singular order near the notch vertex. If exact preservation of the leading local Williams vector field is desired, the corner part may be multiplied by the normalised factors $D_U/D_U(\xi_0,\eta_0)$and $D_V/D_V(\xi_0,\eta_0)$, respectively, so that both multipliers are equal to unity at the notch vertex.

To evaluate the corner functions, the local polar coordinates are related to the global Cartesian coordinates by,

$$r = [(x - x_0)^2 + (y - y_0)^2]^{1/2} = [(x - a + d)^2 + (y - c)^2]^{1/2} \tag{25}$$

$$\theta = \operatorname{atan2}(y - y_0, x_0 - x) = \operatorname{atan2}(y - c, a - d - x) \tag{26}$$

Here, $\text{atan2}(Y, X)$ denotes the four-quadrant inverse tangent, which returns the angle measured from the positive X-axis to the vector (X, Y). Equivalently, expressing Eqs. (25)-(26) in the non-dimensional coordinates gives

$$r = \frac{1}{2}[a^2(\xi - \xi_0)^2 + b^2(\eta - \eta_0)^2]^{1/2} \tag{27}$$

$$\theta = \text{atan2}[b(\eta - \eta_0), a(\xi_0 - \xi)] \tag{28}$$

2.3 Ritz equations and calculation

Collect all unknown Ritz coefficients, namely, A_{mn} ($m = 1, \dots, M$; $n = 1, \dots, N$), B_{mn}, $C_n^{(A)}$ ($n = 1, \dots, N_A$), and $C_n^{(S)}$ ($n = 1, \dots, N_S$), into the single vector

$$\boldsymbol{g} = [\boldsymbol{A}^\top, \boldsymbol{B}^\top, \boldsymbol{C}^{(A)\top}, \boldsymbol{C}^{(S)\top}]^\top \tag{29}$$

where $\boldsymbol{A} = \{A_{mn}\}$, $\boldsymbol{B} = \{B_{mn}\}$, $\boldsymbol{C}^{(A)} = \{C_n^{(A)}\}$, and $\boldsymbol{C}^{(S)} = \{C_n^{(S)}\}$. Substituting Eq. (24) into Eqs. (4)-(5) and applying the stationarity condition $\partial(\mathcal{U}_{\max} - \mathcal{T}_{\max})/\partial\boldsymbol{g} = \boldsymbol{0}$ yields the generalized eigenvalue problem

$$(\boldsymbol{K} - \omega^2\boldsymbol{M})\boldsymbol{g} = \boldsymbol{0} \tag{30}$$

The stiffness matrix adopts the partitioned form

$$\boldsymbol{K} = \begin{bmatrix} \boldsymbol{K}_{pp} & \boldsymbol{K}_{pc} \\ \boldsymbol{K}_{cp} & \boldsymbol{K}_{cc} \end{bmatrix}, \qquad \boldsymbol{K}_{cp} = \boldsymbol{K}_{pc}^\top \tag{31}$$

separating the regular (p) and corner-enriched (c) contributions. The regular-regular block further splits as

$$\boldsymbol{K}_{pp} = \begin{bmatrix} \boldsymbol{K}_{pp,uu} & \boldsymbol{K}_{pp,uv} \\ \boldsymbol{K}_{pp,vu} & \boldsymbol{K}_{pp,vv} \end{bmatrix} \tag{32}$$

Each corner coefficient $C_n^{(q)}$ ($q = A, S$) enters both displacement components simultaneously through $U_{x,n}^{(q)}$ and $U_{y,n}^{(q)}$ in Eq. (24). Consequently, the corner-corner block and the coupling block each receive contributions from both U and V:

$$\boldsymbol{K}_{cc} = \begin{bmatrix} \boldsymbol{K}_{cc,AA} & \boldsymbol{K}_{cc,AS} \\ \boldsymbol{K}_{cc,SA} & \boldsymbol{K}_{cc,SS} \end{bmatrix}, \qquad \boldsymbol{K}_{pc} = \begin{bmatrix} \boldsymbol{K}_{pc,u^A} & \boldsymbol{K}_{pc,u^S} \\ \boldsymbol{K}_{pc,v^A} & \boldsymbol{K}_{pc,v^S} \end{bmatrix} \tag{33}$$

where, for example, $\boldsymbol{K}_{pc,u^A}$ (of size $MN \times N_A$) couples the U-regular basis to the antisymmetric corner coefficients, and $\boldsymbol{K}_{pc,v^A}$ couples the V-regular basis to the same coefficients. Therefore, the full stiffness matrix can be written as

$$\boldsymbol{K} = \begin{bmatrix} \boldsymbol{K}_{pp,uu} & \boldsymbol{K}_{pp,uv} & \boldsymbol{K}_{pc,u^A} & \boldsymbol{K}_{pc,u^S} \\ \boldsymbol{K}_{pp,vu} & \boldsymbol{K}_{pp,vv} & \boldsymbol{K}_{pc,v^A} & \boldsymbol{K}_{pc,v^S} \\ \boldsymbol{K}_{cp,u^A} & \boldsymbol{K}_{cp,v^A} & \boldsymbol{K}_{cc,AA} & \boldsymbol{K}_{cc,AS} \\ \boldsymbol{K}_{cp,u^S} & \boldsymbol{K}_{cp,v^S} & \boldsymbol{K}_{cc,SA} & \boldsymbol{K}_{cc,SS} \end{bmatrix} \tag{34}$$

with $\boldsymbol{K}_{pp,vu} = (\boldsymbol{K}_{pp,uv})^\top$, $\boldsymbol{K}_{cp,u^A} = (\boldsymbol{K}_{pc,u^A})^\top$, $\boldsymbol{K}_{cc,SA} = (\boldsymbol{K}_{cc,AS})^\top$, and analogous relations for the remaining off-diagonal blocks.

The mass matrix follows an identical partitioning. Since U and V enter Eq. (5) independently, $\boldsymbol{M}_{pp}$ is block diagonal

$$\boldsymbol{M} = \begin{bmatrix} \boldsymbol{M}_{pp} & \boldsymbol{M}_{pc} \\ \boldsymbol{M}_{cp} & \boldsymbol{M}_{cc} \end{bmatrix}, \qquad \boldsymbol{M}_{pp} = \begin{bmatrix} \boldsymbol{M}_{pp,uu} & \boldsymbol{0} \\ \boldsymbol{0} & \boldsymbol{M}_{pp,vv} \end{bmatrix} \tag{35}$$

whereas $\boldsymbol{M}_{pc}$ and $\boldsymbol{M}_{cc}$ each receive contributions from both U and V. The full mass matrix can be written as

$$\boldsymbol{M} = \begin{bmatrix} \boldsymbol{M}_{pp,uu} & \boldsymbol{0} & \boldsymbol{M}_{pc,u^A} & \boldsymbol{M}_{pc,u^S} \\ \boldsymbol{0} & \boldsymbol{M}_{pp,vv} & \boldsymbol{M}_{pc,v^A} & \boldsymbol{M}_{pc,v^S} \\ \boldsymbol{M}_{cp,u^A} & \boldsymbol{M}_{cp,v^A} & \boldsymbol{M}_{cc,AA} & \boldsymbol{M}_{cc,AS} \\ \boldsymbol{M}_{cp,u^S} & \boldsymbol{M}_{cp,v^S} & \boldsymbol{M}_{cc,SA} & \boldsymbol{M}_{cc,SS} \end{bmatrix} \tag{36}$$

with $\boldsymbol{M}_{cp,u^A} = (\boldsymbol{M}_{pc,u^A})^\top$, $\boldsymbol{M}_{cc,SA} = (\boldsymbol{M}_{cc,AS})^\top$, and analogous relations for the remaining off-diagonal blocks. The detailed expressions of matrix entries for $\boldsymbol{K}$ and $\boldsymbol{M}$ are presented in Section 2 of the supplementary material.

All integrals are evaluated over the physical domain Ω. For regular-regular terms, one may either integrate directly using Gaussian quadrature on a triangular mesh that covers the notched plate region, or compute the full-rectangle contribution and subtract the triangular notch contribution. For coupling and corner-corner terms, direct quadrature over the physical domain is applied. The plate domain is first triangulated, with the triangular notch excluded from the mesh. A degree-19 Gaussian quadrature rule providing 73 integration points per triangle [31] is applied on each element. To accurately resolve the singular behaviour of the corner functions near the notch vertex, triangles whose vertices fall within a prescribed radius of the vertex are further subdivided by bisecting each edge, yielding a locally refined mesh. At each Gauss point, r and θ are evaluated from Eqs. (27)-(28), and the derivatives Eqs. (B.15)-(B.16) are computed directly; the corner functions and their gradients follow from Eqs. (B.17)-(B.19) without further coordinate transformation.

After assembling $\boldsymbol{K}$ and $\boldsymbol{M}$, the natural frequencies and mode shapes are obtained from the non-trivial solutions of

$$|\boldsymbol{K} - \omega^2 \boldsymbol{M}| = 0 \tag{37}$$

yielding the squared natural frequencies ω_i^2 and the eigenvectors $\boldsymbol{g}_i$. The corresponding mode shapes are reconstructed by substituting the components of $\boldsymbol{g}_i$ into Eq. (24), giving the modal displacement fields $U_i(\xi, \eta)$ and $V_i(\xi, \eta)$ over Ω. Mode shapes are normalized with respect to the maximum in-plane displacement magnitude.

3 Convergence studies

The convergence of the proposed formulation is examined first for intact plates, and then for plates under various boundary conditions with a horizontal or vertical V-notch, by increasing the numbers of regular terms M and N and the numbers of retained antisymmetric and symmetric Williams corner functions N_A and N_S. In the present calculations, a square truncation scheme with $M = N$ and $N_A = N_S$ is adopted for simplicity. The results are validated by comparing with published solutions or finite element results. A Poisson's ratio of 0.3 is considered for all the results shown hereafter. The boundary conditions for a rectangular plate are denoted by four letters, referring to the left edge, bottom edge, right edge, and top edge, respectively. Letters C and F represent clamped and free boundary conditions, respectively. There are two definitions of in-plane simply supported edges, denoted here as S_1 and S_2. An S_1-type edge corresponds to zero displacement parallel to the edge and zero normal stress perpendicular to the edge, whereas the S_2-type edge corresponds to zero displacement normal to the edge and zero shear stress along the edge.

Table 1 gives the first eight frequency parameters of intact rectangular plates under selected boundary conditions. Results with respect to $M = N =$4, 6, 8, 10, 12, and 14 are listed. Comparison with exact solutions [12] and solutions obtained using the Ritz method [14] and the superposition method [32] is also presented. It can be observed that the frequency parameters converge rapidly and monotonically from above to the reported precision as $M = N$ increases, with changes beyond $M = N = 10$ confined to the fourth decimal place. Increasing $M = N$ beyond 10 produces only very small changes in the reported digits. In all cases, the current results are in excellent agreement with those in the literature. These comparisons confirm the accuracy of the current formulation for the solutions without corner functions, and that the upper-bound characteristic of the Ritz solution has been maintained.

Table 1. Convergence studies of frequency parameters for intact rectangular plates.

Boundary conditions	$M = N$	Mode No.							
		1	2	3	4	5	6	7	8
Frequency parameters $(\omega a/\pi)\sqrt{2\rho(1+\nu)/E}$; Aspect ratio $b/a = 1.2$									
S_1CS_1C	4	0.8333	1.5408	1.6672	1.7854	2.3354	2.4027	2.6455	2.6807
	6	0.8333	1.5406	1.6667	1.7846	2.2493	2.3915	2.5004	2.5735
	8	0.8333	1.5406	1.6667	1.7846	2.2493	2.3915	2.5000	2.5735
	10	0.8333	1.5406	1.6667	1.7846	2.2493	2.3915	2.5000	2.5735
	12	0.8333	1.5406	1.6667	1.7846	2.2493	2.3915	2.5000	2.5735
	14	0.8333	1.5406	1.6667	1.7846	2.2493	2.3915	2.5000	2.5735
	Xing and Liu [12]	0.8333	1.5406	1.6667	1.7846	2.2493	2.3915	2.5000	2.5735
S_2FS_2F	4	0.8016	1.2765	1.4090	1.7419	1.8004	2.2906	2.3518	2.8280
	6	0.7975	1.2751	1.4086	1.7285	1.7601	1.7829	1.9268	2.4258
	8	0.7974	1.2751	1.4086	1.7284	1.7600	1.7803	1.9251	2.4209
	10	0.7974	1.2751	1.4086	1.7284	1.7600	1.7800	1.9249	2.4207
	12	0.7974	1.2751	1.4086	1.7284	1.7600	1.7799	1.9249	2.4206
	14	0.7974	1.2751	1.4086	1.7284	1.7600	1.7799	1.9248	2.4206
	Xing and Liu [12]	0.7974	1.2751	1.4086	1.7284	1.7600	1.7799	1.9248	2.4206
S_1CS_2F	4	0.7359	0.9029	1.4031	1.5314	2.0099	2.0513	2.4944	2.5029
	6	0.7359	0.9029	1.3972	1.5252	1.9594	2.0398	2.2932	2.4126
	8	0.7359	0.9029	1.3971	1.5252	1.9594	2.0398	2.2924	2.4121
	10	0.7359	0.9029	1.3971	1.5252	1.9594	2.0398	2.2923	2.4121
	12	0.7359	0.9029	1.3971	1.5252	1.9594	2.0398	2.2923	2.4121
	14	0.7359	0.9029	1.3971	1.5252	1.9594	2.0398	2.2923	2.4121

	Xing and Liu [12]	0.7359	0.9029	1.3971	1.5252	1.9594	2.0398	2.2923	2.4121
Frequency parameters $\omega a\sqrt{\rho(1-\nu^2)/E}$; Aspect ratio $b/a = 1.0$									
$CCCC$	4	3.5556	3.5556	4.2382	5.2026	5.8784	6.1399	6.1399	6.7344
	6	3.5553	3.5553	4.2350	5.1860	5.8587	5.8949	5.8949	6.7083
	8	3.5552	3.5552	4.2350	5.1858	5.8586	5.8944	5.8944	6.7079
	10	3.5552	3.5552	4.2350	5.1857	5.8586	5.8944	5.8944	6.7078
	12	3.5552	3.5552	4.2350	5.1857	5.8586	5.8944	5.8944	6.7077
	14	3.5552	3.5552	4.2350	5.1857	5.8586	5.8944	5.8944	6.7077
	Dozio [14]	3.5552	3.5552	4.2350	5.1859	5.8587	5.8946	5.8946	6.7080
$FFFF$	4	2.3553	2.6198	2.6198	2.6364	3.0454	3.4711	4.3337	4.3337
	6	2.3212	2.4729	2.4729	2.6286	2.9879	3.4524	3.7249	3.7249
	8	2.3207	2.4718	2.4718	2.6285	2.9874	3.4523	3.7233	3.7233
	10	2.3206	2.4717	2.4717	2.6284	2.9874	3.4522	3.7232	3.7232
	12	2.3206	2.4716	2.4716	2.6284	2.9874	3.4522	3.7231	3.7231
	14	2.3206	2.4716	2.4716	2.6284	2.9874	3.4522	3.7231	3.7231
	Dozio [14]	2.3206	2.4716	2.4716	2.6284	2.9874	3.4522	3.7232	3.7232
Frequency parameters $(\omega a/2)\sqrt{\rho(1-\nu^2)/E}$; Aspect ratio $b/a = 1.0$									
$S_2S_2S_2S_2$	4	1.3144	1.5708	1.5708	2.2215	2.3936	2.3936	2.9760	3.1425
	6	1.3142	1.5708	1.5708	2.0780	2.0780	2.2214	2.6284	2.9519
	8	1.3142	1.5708	1.5708	2.0780	2.0780	2.2214	2.6284	2.9389
	10	1.3142	1.5708	1.5708	2.0780	2.0780	2.2214	2.6284	2.9387
	12	1.3142	1.5708	1.5708	2.0780	2.0780	2.2214	2.6284	2.9387
	14	1.3142	1.5708	1.5708	2.0780	2.0780	2.2214	2.6284	2.9387
	Gorman [32]	1.314	1.571	1.571	2.078	2.078	2.221	2.629	2.939

The convergence of V-notched solutions is investigated in Table 2-Table 6. Since no published result is available for comparison, the commercial finite element software ANSYS Mechanical APDL is used to calculate dimensionless frequency parameters under the same conditions. The ANSYS results are obtained using two-dimensional elements PLANE183. The KSCON command is employed to account for the crack tip singularity and refine the mesh near the crack tip. Convergence studies are performed on the ANSYS model to ensure the obtained results converge to the second decimal place. Table 2-Table 4 examine convergence for a S_1CFS_2 square plate with a horizontal V-notch ($c/b = 0.6$, $d/a = 0.15$, $\gamma = 90^{\circ}$), a $S_1S_2S_2F$ square plate with a vertical V-notch ($c/a = 0.7$, $d/b = 0.25$, $\gamma = 60^{\circ}$), and a $CCFC$ square plate with a horizontal V-notch ($c/b = 0.5$, $d/a = 0.2$, $\gamma = 45^{\circ}$). Each table contrasts the unenriched solution ($N_A = N_S = 0$) with the enriched one. It should be mentioned that $N_A = N_S = 0$ still represents the physical V-notched domain. It denotes a calculation in which the displacement field is represented using only the regular admissible functions, without local corner enrichment, and the recognition of the existence of the V-notch is only through the integration domain. For the notch angles considered, namely, $\gamma = 90^{\circ}$, 60°, and 45°, each characteristic equation (i.e. Eqs. (19)-(20)) has only one retained positive root after $\lambda = 1$ is excluded. Both retained roots satisfy $0 < \lambda < 1$ and therefore describe singular stress fields at the notch vertex. Thus, $N_A = N_S = 1$ in Table 2-Table 4 represents the complete available Williams enrichment for these three cases rather than an arbitrarily selected truncation.

Table 2 considers a relatively wide and shallow notch. The regular approximation alone gives steadily convergent results, and the inclusion of the corner functions produces only a moderate improvement to the convergence. The two solutions converge to very close values. For example, the fourth frequency parameter at $M = N = 4$ decreases from 1.716 without enrichment to 1.700 with enrichment, while the converged value is approximately 1.693. This behaviour indicates that the global regular functions can represent this relatively mild geometric discontinuity reasonably well, although the corner functions reduce the number of regular terms required and accelerates the convergence.

Table 2. Convergence of frequency parameters $(\omega a/2)\sqrt{\rho(1-\nu^2)/E}$ for a S_1CFS_2 square plate with a horizontal V-notch ($c/b = 0.6$, $d/a = 0.15$, $\gamma = 90^{\circ}$).

Mode No.	$N_A = N_S$	$M = N$												ANSYS results
		4	6	8	10	12	14	16	⋯	32	34	36	38	
1	0	0.429	0.428	0.428	0.427	0.427	0.427	0.427	⋯	0.426	0.426	0.426	0.426	0.426

	1	0.428	0.427	0.426	0.426	0.426	0.426	0.426	⋯	0.426	0.426	0.426	0.426	
2	0	1.294	1.285	1.283	1.281	1.280	1.279	1.279	⋯	1.278	1.278	1.278	1.278	1.279
	1	1.287	1.279	1.278	1.278	1.278	1.278	1.278	⋯	1.278	1.278	1.278	1.278	
3	0	1.410	1.409	1.408	1.408	1.407	1.407	1.407	⋯	1.406	1.406	1.406	1.406	1.411
	1	1.409	1.407	1.407	1.406	1.406	1.406	1.406	⋯	1.406	1.406	1.406	1.406	
4	0	1.716	1.707	1.704	1.701	1.700	1.699	1.698	⋯	1.695	1.695	1.695	1.695	1.694
	1	1.700	1.696	1.695	1.695	1.694	1.694	1.694	⋯	1.693	1.693	1.693	1.693	
5	0	1.890	1.865	1.860	1.857	1.855	1.853	1.852	⋯	1.847	1.847	1.847	1.847	1.846
	1	1.878	1.852	1.849	1.848	1.847	1.846	1.846	⋯	1.845	1.845	1.845	1.845	
6	0	2.147	2.082	2.070	2.061	2.056	2.053	2.051	⋯	2.044	2.043	2.043	2.043	2.043
	1	2.107	2.050	2.046	2.044	2.043	2.042	2.042	⋯	2.040	2.040	2.040	2.040	
7	0	2.370	2.204	2.196	2.191	2.189	2.187	2.186	⋯	2.183	2.183	2.183	2.183	2.185
	1	2.340	2.186	2.184	2.183	2.182	2.182	2.182	⋯	2.181	2.181	2.181	2.181	
8	0	2.616	2.465	2.461	2.459	2.458	2.457	2.456	⋯	2.455	2.455	2.455	2.455	2.457
	1	2.611	2.456	2.455	2.455	2.455	2.455	2.454	⋯	2.454	2.454	2.454	2.454	

The benefit of the enrichment becomes more evident in Table 3 and Table 4 as the notch angle decreases and the local vertex behaviour becomes more pronounced. In Table 3, the second frequency parameter obtained with $M = N = 16$ changes from 0.754 for $N_A = N_S = 0$ to 0.730 for $N_A = N_S = 1$, compared with the ANSYS result of 0.727. In Table 4, the fifth frequency parameter remains at 2.154 even at $M = N = 50$ when only regular functions are used, whereas the enriched solution stabilises at approximately 2.125, close to the ANSYS result of 2.129. The influence of the enrichment is mode dependent, since different modal displacement and stress fields interact differently with the notch vertex. Nevertheless, the overall results demonstrate that incorporating the singular corner functions can substantially accelerate convergence for the notch sensitive modes. This is also reflected in the singularity strength across Table 2-Table 4. As γ decreases from 90° to 45°, $\lambda^{(A)}$ falls from 0.9085 to 0.6597 and $\lambda^{(S)}$ from 0.5445 to 0.5050, the stress field $r^{\lambda-1}$ becomes more strongly singular, and the regular admissible functions become correspondingly less able to reproduce it. The two corner functions supply exactly the missing content, thus convergence accelerates with the strength of the singularity.

Table 3. Convergence of frequency parameters $(\omega a/2)\sqrt{\rho(1-\nu^2)/E}$ for a $S_1S_2S_2F$ square plate with a vertical V-notch ($c/a = 0.7$, $d/b = 0.25$, $\gamma = 60^{\circ}$).

Mode No.	$N_A = N_S$	$M = N$												ANSYS results
		4	6	8	10	12	14	16	⋯	28	30	32	34	
1	0	0.673	0.673	0.671	0.670	0.669	0.668	0.667	⋯	0.663	0.663	0.663	0.662	0.659
	1	0.666	0.663	0.661	0.661	0.660	0.659	0.659	⋯	0.658	0.658	0.658	0.658	
2	0	0.816	0.808	0.788	0.777	0.766	0.758	0.754	⋯	0.739	0.738	0.737	0.737	0.727
	1	0.747	0.739	0.735	0.733	0.731	0.730	0.730	⋯	0.728	0.728	0.728	0.728	
3	0	1.281	1.275	1.270	1.266	1.263	1.261	1.259	⋯	1.255	1.254	1.254	1.254	1.252
	1	1.259	1.255	1.254	1.253	1.253	1.253	1.252	⋯	1.252	1.252	1.252	1.252	
4	0	1.302	1.295	1.287	1.280	1.276	1.273	1.271	⋯	1.268	1.267	1.267	1.267	1.267
	1	1.285	1.271	1.268	1.267	1.267	1.266	1.266	⋯	1.265	1.265	1.265	1.265	
5	0	2.008	1.886	1.873	1.862	1.855	1.849	1.846	⋯	1.838	1.837	1.837	1.836	1.833
	1	2.005	1.840	1.838	1.836	1.835	1.835	1.834	⋯	1.833	1.833	1.833	1.833	
6	0	2.183	1.986	1.985	1.985	1.985	1.984	1.984	⋯	1.983	1.983	1.983	1.983	1.988
	1	2.081	1.984	1.983	1.983	1.983	1.983	1.983	⋯	1.983	1.983	1.983	1.983	
7	0	2.314	2.127	2.111	2.095	2.088	2.083	2.080	⋯	2.075	2.075	2.074	2.074	2.073
	1	2.198	2.080	2.077	2.075	2.074	2.074	2.073	⋯	2.072	2.072	2.072	2.072	
8	0	2.436	2.423	2.419	2.416	2.414	2.413	2.412	⋯	2.408	2.408	2.408	2.408	2.412
	1	2.424	2.410	2.408	2.407	2.406	2.406	2.406	⋯	2.405	2.405	2.405	2.405	

Table 4. Convergence of frequency parameters $(\omega a/2)\sqrt{\rho(1-\nu^2)/E}$ for a $CCFC$ square plate with a horizontal V-notch ($c/b = 0.5$, $d/a = 0.2$, $\gamma = 45^{\circ}$).

Mode No.	$N_A = N_S$	$M = N$												ANSYS results
		4	6	8	10	12	14	16	⋯	44	46	48	50	

1	0	1.172	1.168	1.165	1.163	1.160	1.157	1.155	⋯	1.145	1.145	1.144	1.144	1.144
	1	1.150	1.146	1.145	1.144	1.143	1.143	1.142	⋯	1.141	1.141	1.141	1.141	
2	0	1.618	1.616	1.615	1.614	1.614	1.614	1.614	⋯	1.613	1.613	1.613	1.613	1.618
	1	1.618	1.615	1.614	1.613	1.613	1.613	1.613	⋯	1.612	1.612	1.612	1.612	
3	0	1.750	1.743	1.740	1.738	1.735	1.733	1.731	⋯	1.719	1.719	1.719	1.719	1.721
	1	1.732	1.725	1.722	1.720	1.719	1.719	1.718	⋯	1.716	1.716	1.716	1.716	
4	0	2.187	2.161	2.158	2.155	2.153	2.150	2.147	⋯	2.131	2.131	2.130	2.130	2.103
	1	2.168	2.141	2.136	2.133	2.129	2.123	2.120	⋯	2.104	2.103	2.103	2.103	
5	0	2.449	2.436	2.433	2.432	2.408	2.365	2.327	⋯	2.163	2.160	2.156	2.154	2.129
	1	2.258	2.169	2.146	2.135	2.131	2.130	2.129	⋯	2.125	2.125	2.125	2.125	
6	0	2.611	2.538	2.501	2.457	2.433	2.432	2.432	⋯	2.430	2.430	2.430	2.430	2.432
	1	2.454	2.436	2.434	2.432	2.432	2.431	2.431	⋯	2.430	2.430	2.430	2.430	
7	0	2.725	2.541	2.535	2.533	2.531	2.529	2.527	⋯	2.511	2.510	2.510	2.510	2.507
	1	2.606	2.523	2.517	2.513	2.511	2.510	2.509	⋯	2.505	2.504	2.504	2.504	
8	0	3.007	2.946	2.929	2.914	2.900	2.887	2.877	⋯	2.818	2.817	2.815	2.814	2.791
	1	2.947	2.834	2.821	2.814	2.808	2.803	2.799	⋯	2.786	2.785	2.785	2.785	

Table 5 considers a $CFFF$ square plate with a sharper horizontal notch ($c/b = 0.6, d/a = 0.2, \gamma = 15^{\circ}$). For this angle, the characteristic equations provide additional positive roots above unity. The first retained root in each family satisfies $0 < \lambda < 1$ and represents the singular part of the local field, whereas the subsequent roots with $\lambda > 1$ describe progressively smoother higher order terms. The dominant contribution is obtained by introducing the first root. This is particularly clear for the fourth mode: at $M = N = 40$, the unenriched solution gives 1.202, while the inclusion of one root from each family gives 0.847, in close agreement with the ANSYS result of 0.846. The regular approximation is therefore converging extremely slowly for this mode, and incorporating the corner functions corresponding to the singular roots can substantially improve the convergence.

Further increases in $N_A = N_S$ produce smaller corrections. For most modes in Table 5, the results obtained using four and five roots agree to the reported three decimal places. The first singular root therefore captures the leading local behaviour, while the additional roots provide progressively smaller refinements to the surrounding displacement field. The results also show that the number of corner functions required is mode dependent. The lower modes that are weakly affected by the notch stabilise with only one or two roots, whereas some higher or more notch sensitive modes require additional terms.

Table 5. Convergence of frequency parameters $(\omega a/2)\sqrt{\rho(1-\nu^2)/E}$ for a $CFFF$ square plate with a horizontal V-notch ($c/b = 0.6$, $d/a = 0.2$, $\gamma = 15^{\circ}$).

Mode No.	$N_A = N_S$	$M = N$												ANSYS results
		4	6	8	10	12	14	16	⋯	34	36	38	40	
1	0	0.318	0.316	0.316	0.316	0.316	0.316	0.316	⋯	0.316	0.316	0.316	0.316	0.315
	1	0.318	0.316	0.316	0.316	0.316	0.316	0.315	⋯	0.315	0.315	0.315	0.315	
	2	0.317	0.316	0.316	0.316	0.316	0.316	0.315	⋯	0.315	0.315	0.315	0.315	
	3	0.317	0.316	0.316	0.316	0.316	0.316	0.315	⋯	0.315	0.315	0.315	0.315	
	4	0.317	0.316	0.316	0.316	0.315	0.315	0.315	⋯	0.315	0.315	0.315	0.315	
	5	0.317	0.316	0.316	0.316	0.315	0.315	0.315	⋯	0.315	0.315	0.315	0.315	
2	0	0.759	0.758	0.758	0.758	0.757	0.757	0.757	⋯	0.757	0.757	0.757	0.757	0.754
	1	0.758	0.757	0.756	0.756	0.756	0.756	0.755	⋯	0.755	0.755	0.755	0.755	
	2	0.757	0.757	0.756	0.756	0.755	0.755	0.755	⋯	0.755	0.755	0.755	0.755	
	3	0.757	0.756	0.756	0.756	0.755	0.755	0.755	⋯	0.755	0.755	0.755	0.755	
	4	0.757	0.756	0.756	0.755	0.755	0.755	0.755	⋯	0.755	0.755	0.754	0.754	
	5	0.757	0.756	0.756	0.755	0.755	0.755	0.755	⋯	0.755	0.754	0.754	0.754	
3	0	0.850	0.847	0.846	0.846	0.846	0.846	0.846	⋯	0.846	0.846	0.846	0.846	0.816
	1	0.849	0.846	0.845	0.845	0.844	0.844	0.842	⋯	0.830	0.830	0.829	0.828	
	2	0.849	0.846	0.845	0.844	0.843	0.842	0.840	⋯	0.829	0.828	0.828	0.827	
	3	0.849	0.846	0.845	0.844	0.843	0.841	0.840	⋯	0.829	0.828	0.827	0.827	
	4	0.848	0.845	0.843	0.841	0.838	0.836	0.834	⋯	0.826	0.826	0.825	0.825	
	5	0.848	0.845	0.843	0.841	0.838	0.836	0.834	⋯	0.826	0.826	0.825	0.825	

4	0	1.376	1.324	1.322	1.319	1.316	1.313	1.309	···	1.239	1.227	1.215	1.202	0.846
	1	0.970	0.917	0.886	0.873	0.863	0.857	0.853	···	0.847	0.847	0.847	0.847	
	2	0.929	0.893	0.872	0.863	0.856	0.853	0.850	···	0.847	0.847	0.847	0.847	
	3	0.915	0.880	0.865	0.859	0.854	0.852	0.850	···	0.847	0.847	0.847	0.847	
	4	0.892	0.865	0.856	0.852	0.849	0.849	0.848	···	0.847	0.847	0.847	0.847	
	5	0.891	0.864	0.855	0.851	0.849	0.848	0.848	···	0.847	0.847	0.847	0.847	
5	0	1.483	1.451	1.450	1.449	1.449	1.449	1.448	···	1.445	1.444	1.444	1.443	1.411
	1	1.472	1.437	1.433	1.431	1.429	1.427	1.426	···	1.419	1.419	1.419	1.418	
	2	1.469	1.436	1.432	1.429	1.427	1.426	1.425	···	1.419	1.419	1.419	1.418	
	3	1.460	1.435	1.432	1.429	1.427	1.426	1.425	···	1.419	1.419	1.418	1.418	
	4	1.454	1.427	1.423	1.422	1.421	1.420	1.420	···	1.417	1.416	1.416	1.416	
	5	1.453	1.426	1.423	1.421	1.420	1.419	1.418	···	1.416	1.415	1.415	1.415	
6	0	1.549	1.536	1.536	1.536	1.536	1.535	1.535	···	1.532	1.531	1.531	1.530	1.511
	1	1.544	1.519	1.518	1.518	1.518	1.518	1.517	···	1.516	1.516	1.515	1.515	
	2	1.543	1.519	1.518	1.518	1.518	1.517	1.517	···	1.514	1.514	1.514	1.514	
	3	1.542	1.517	1.516	1.515	1.514	1.514	1.514	···	1.512	1.512	1.512	1.512	
	4	1.540	1.517	1.515	1.514	1.514	1.513	1.513	···	1.512	1.512	1.512	1.512	
	5	1.538	1.517	1.515	1.514	1.514	1.513	1.513	···	1.512	1.512	1.512	1.512	
7	0	2.078	1.936	1.933	1.932	1.932	1.931	1.930	···	1.918	1.917	1.914	1.912	1.832
	1	2.051	1.890	1.880	1.874	1.870	1.866	1.862	···	1.848	1.847	1.847	1.846	
	2	2.041	1.885	1.875	1.869	1.864	1.861	1.859	···	1.847	1.846	1.846	1.845	
	3	2.026	1.882	1.873	1.867	1.863	1.860	1.857	···	1.846	1.846	1.845	1.844	
	4	2.025	1.861	1.853	1.850	1.849	1.848	1.846	···	1.841	1.841	1.840	1.840	
	5	1.979	1.860	1.851	1.848	1.846	1.845	1.844	···	1.839	1.839	1.839	1.839	
8	0	2.176	2.053	2.049	2.048	2.048	2.047	2.047	···	2.044	2.043	2.043	2.042	2.035
	1	2.158	2.045	2.040	2.039	2.038	2.038	2.038	···	2.037	2.037	2.037	2.037	
	2	2.158	2.045	2.040	2.039	2.038	2.038	2.037	···	2.036	2.036	2.036	2.036	

	3	2.157	2.042	2.038	2.037	2.036	2.036	2.036	···	2.035	2.035	2.035	2.035	
	4	2.157	2.042	2.038	2.037	2.036	2.036	2.036	···	2.035	2.035	2.035	2.035	
	5	2.157	2.042	2.038	2.036	2.036	2.036	2.036	···	2.035	2.035	2.035	2.035	

The very sharp notch with $\gamma = 5°$considered in Table 6 for a free square plate admits many positive Williams roots (namely, 21 antisymmetric roots excluding $\lambda^{(A)} = 1$ and 23 symmetric roots), however, it is unnecessary to include all of them. The addition of the first root again produces the largest change in the results. For example, the first frequency parameter at $M = N = 50$ decreases from 1.160 without enrichment to 1.086 with one root and to 1.082 with four roots, compared with the ANSYS result of 1.078. By contrast, several other modes become effectively insensitive to N_A and N_S after the first or second root is introduced. The first mode is the most demanding case and therefore dominates the enrichment and regular terms required for this configuration.

Although additional positive roots are still admissible, retaining an excessive number of them can impair numerical conditioning. As λ increases, the functions proportional to r^{λ} become increasingly smooth near the notch vertex. Their behaviour can then be represented partly by the regular admissible functions, causing the regular and corner bases to become possibly linear-dependent. The resulting stiffness and mass matrices may therefore become ill-conditioned, and the computed eigenvalues become increasingly sensitive to numerical integration and round-off errors. For example, without showing the results in Table 6, when $N_A = N_S = 7$, ill-conditioning occurs when $M = N \geq 16$. Therefore, the retained number of corner functions should be determined from the observed monotonicity or stabilization of frequency parameters rather than from the total number of available roots.

Table 6. Convergence of frequency parameters $(\omega a/2)\sqrt{\rho(1-\nu^2)/E}$ for a free square plate with a vertical V-notch ($c/a = 0.5$, $d/b = 0.1$, $\gamma = 5^{\circ}$).

Mode No.	$N_A = N_S$	$M = N$												ANSYS results
		4	6	8	10	12	14	16	···	44	46	48	50	
1	0	1.178	1.161	1.160	1.160	1.160	1.160	1.160	···	1.160	1.160	1.160	1.160	1.078
	1	1.178	1.152	1.135	1.126	1.121	1.115	1.110	···	1.088	1.087	1.086	1.086	
	2	1.177	1.142	1.127	1.120	1.115	1.110	1.106	···	1.086	1.086	1.085	1.085	
	3	1.174	1.127	1.112	1.107	1.104	1.101	1.098	···	1.085	1.084	1.084	1.084	

	4	1.170	1.110	1.102	1.099	1.097	1.095	1.093	···	1.083	1.082	1.082	1.082	
	0	1.309	1.235	1.235	1.234	1.234	1.234	1.234	···	1.234	1.234	1.234	1.234	
	1	1.227	1.160	1.160	1.160	1.160	1.160	1.160	···	1.160	1.160	1.160	1.160	
2	2	1.199	1.160	1.160	1.160	1.160	1.160	1.160	···	1.160	1.160	1.160	1.160	1.160
	3	1.187	1.160	1.160	1.160	1.160	1.160	1.160	···	1.160	1.160	1.160	1.160	
	4	1.173	1.160	1.160	1.160	1.160	1.160	1.160	···	1.160	1.160	1.160	1.160	
	0	1.310	1.237	1.236	1.236	1.236	1.236	1.236	···	1.236	1.236	1.236	1.236	
	1	1.310	1.236	1.236	1.236	1.236	1.236	1.236	···	1.235	1.235	1.235	1.235	
3	2	1.309	1.236	1.236	1.236	1.236	1.236	1.236	···	1.235	1.235	1.235	1.235	1.235
	3	1.303	1.236	1.236	1.236	1.236	1.236	1.236	···	1.235	1.235	1.235	1.235	
	4	1.298	1.236	1.236	1.236	1.235	1.235	1.235	···	1.235	1.235	1.235	1.235	
	0	1.319	1.315	1.315	1.315	1.315	1.315	1.315	···	1.315	1.315	1.315	1.315	
	1	1.319	1.315	1.315	1.315	1.315	1.315	1.314	···	1.314	1.314	1.314	1.314	
4	2	1.318	1.315	1.315	1.315	1.315	1.315	1.314	···	1.314	1.314	1.314	1.314	1.314
	3	1.318	1.315	1.315	1.315	1.314	1.314	1.314	···	1.314	1.314	1.314	1.314	
	4	1.318	1.315	1.315	1.314	1.314	1.314	1.314	···	1.314	1.314	1.314	1.314	
	0	1.522	1.493	1.493	1.492	1.492	1.492	1.492	···	1.492	1.492	1.492	1.492	
	1	1.492	1.447	1.441	1.439	1.437	1.436	1.434	···	1.429	1.429	1.429	1.429	
5	2	1.489	1.443	1.439	1.437	1.436	1.434	1.433	···	1.429	1.428	1.428	1.428	1.427
	3	1.488	1.439	1.435	1.433	1.432	1.432	1.431	···	1.428	1.428	1.428	1.428	
	4	1.482	1.434	1.432	1.431	1.431	1.430	1.430	···	1.428	1.428	1.428	1.428	
	0	1.736	1.726	1.726	1.726	1.726	1.726	1.726	···	1.726	1.726	1.726	1.726	
	1	1.727	1.714	1.712	1.712	1.711	1.711	1.711	···	1.709	1.709	1.709	1.709	
6	2	1.726	1.713	1.712	1.711	1.711	1.711	1.710	···	1.709	1.709	1.709	1.709	1.708
	3	1.726	1.712	1.711	1.711	1.711	1.711	1.710	···	1.709	1.709	1.709	1.709	
	4	1.723	1.711	1.711	1.710	1.710	1.710	1.710	···	1.709	1.709	1.709	1.709	
7	0	2.166	1.862	1.862	1.862	1.861	1.861	1.861	···	1.861	1.861	1.861	1.861	1.858

	1	2.153	1.861	1.861	1.860	1.860	1.860	1.860	⋯	1.859	1.859	1.859	1.859	
	2	2.129	1.861	1.860	1.860	1.860	1.860	1.860	⋯	1.859	1.859	1.859	1.859	
	3	2.084	1.861	1.860	1.860	1.860	1.860	1.860	⋯	1.859	1.859	1.859	1.859	
	4	2.069	1.861	1.860	1.859	1.859	1.859	1.859	⋯	1.859	1.858	1.858	1.858	
	0	2.167	1.863	1.862	1.862	1.862	1.862	1.862	⋯	1.862	1.862	1.862	1.862	
	1	2.166	1.863	1.862	1.862	1.862	1.862	1.862	⋯	1.862	1.862	1.862	1.862	
8	2	2.138	1.863	1.862	1.862	1.862	1.862	1.862	⋯	1.862	1.862	1.862	1.862	1.862
	3	2.120	1.863	1.862	1.862	1.862	1.862	1.862	⋯	1.862	1.862	1.862	1.862	
	4	2.111	1.863	1.862	1.862	1.862	1.862	1.862	⋯	1.862	1.862	1.862	1.862	

Overall, Table 2-Table 6 demonstrate that the current formulation yields accurate upper-bound solutions. The corner enrichment is most effective for sharp notches and for modes whose local fields are inadequately represented by the regular admissible functions. When only one positive root is available in each family, both roots should be retained. When several roots are available, the leading singular roots provide the principal improvement, while the additional roots should be added only until the frequencies of interest converge.

Based on the preceding convergence studies, for the numerical results hereafter, the regular truncation $M = N = 50$ is adopted. $N_A = N_S = 1$ is used for notch angles admitting only one retained root in each symmetry family, whereas for sharper notches admitting several roots, the number of roots depends on the notch angle, and only the number required to reach converged frequency parameters is retained.

4 Numerical results and discussion

Based on the convergence studies presented in Section 3, the regular truncation is fixed at $M = N = 50$. The corner function truncations are $N_A = N_S = 4$, 5, and 2 for notch angles $\gamma = 5°$, $15°$, and $30°$, respectively. Table 7 and Table 8 present the first eight nonzero frequency parameters and the corresponding in-plane mode shapes of a completely free square plate with a vertical V-notch lying along the centreline. The three rigid body modes are omitted. The intact plate results are also included to provide a reference for assessing the effects of the notch depth and opening angle. Since each mode shape is independently normalised, the contour levels indicate the spatial distribution of the displacement magnitude within a mode and should not be used to compare absolute modal amplitudes between different modes.

Table 7. The frequency parameters $(\omega a/2)\sqrt{\rho(1-\nu^2)/E}$ and mode shapes for a free square plate with a vertical V-notch at $c/a = 0.5$: Mode 1 to Mode 4.

Notch angle γ	d/b	Mode No.			
		1	2	3	4
N/A	0	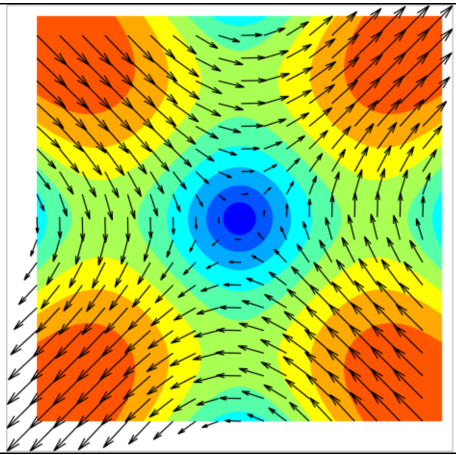	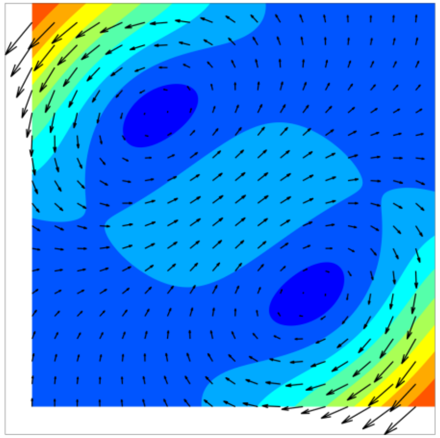	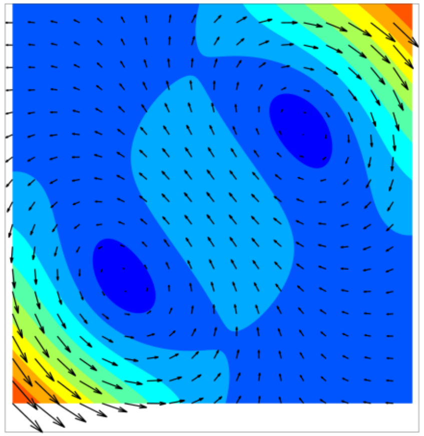	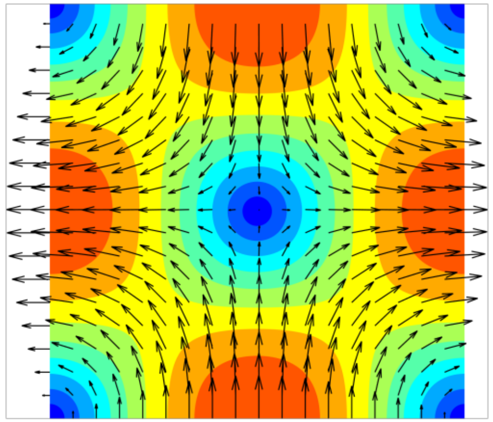
		1.160	1.236	1.236	1.314
5°	0.1	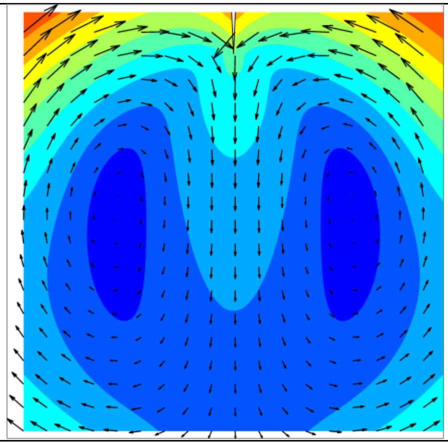	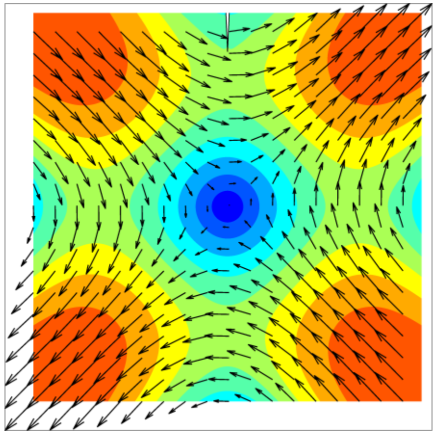	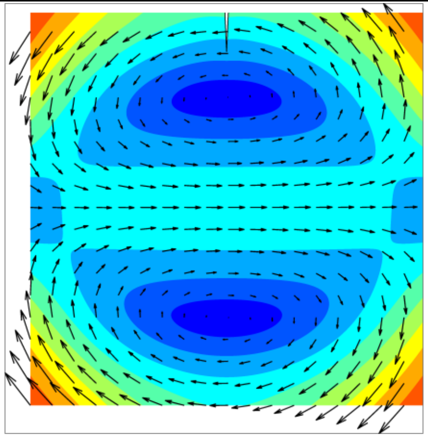	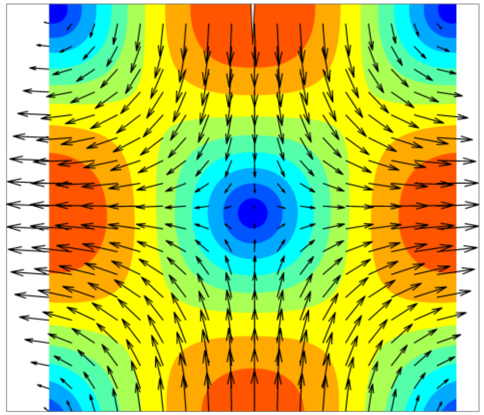

		1.082	1.160	1.235	1.314
	0.3	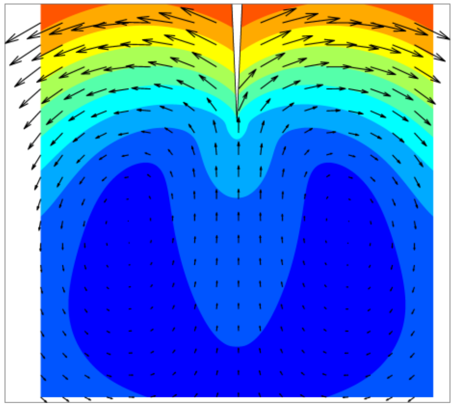	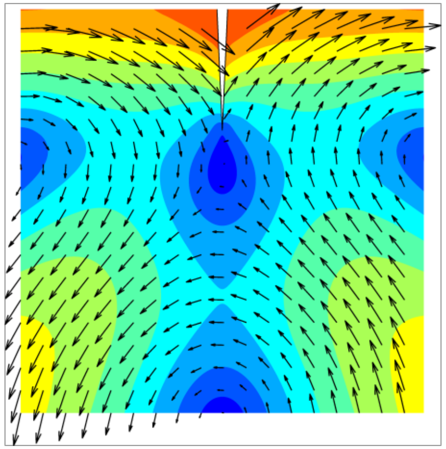	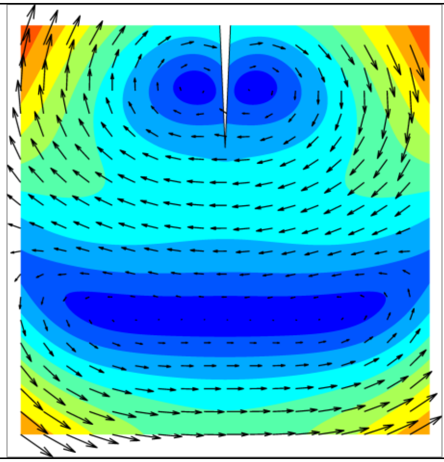	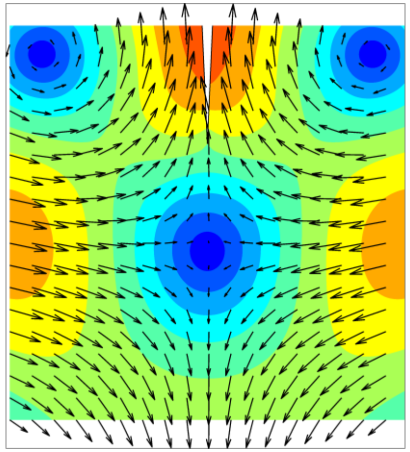
		0.571	1.081	1.214	1.302
	0.5	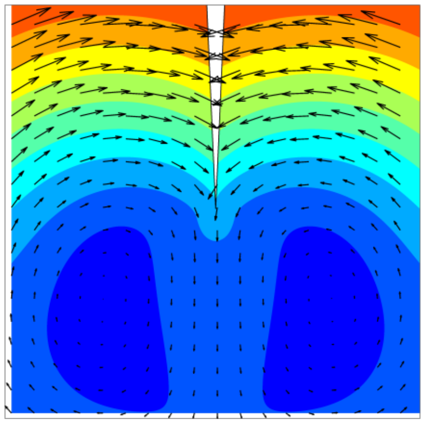	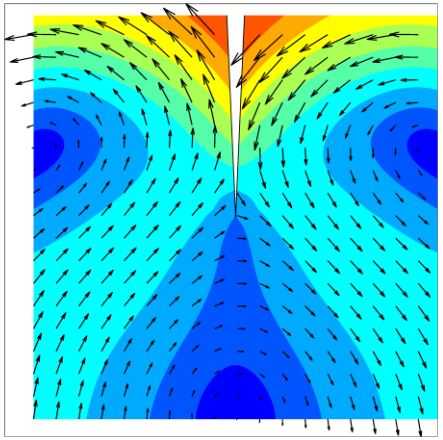	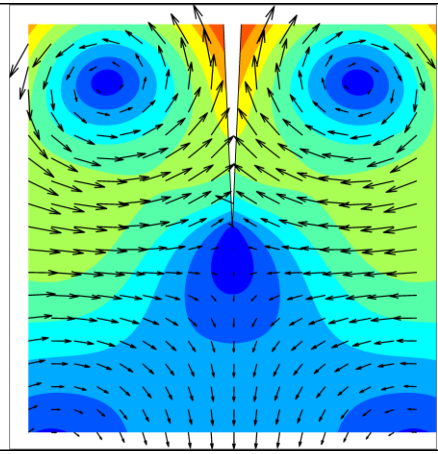	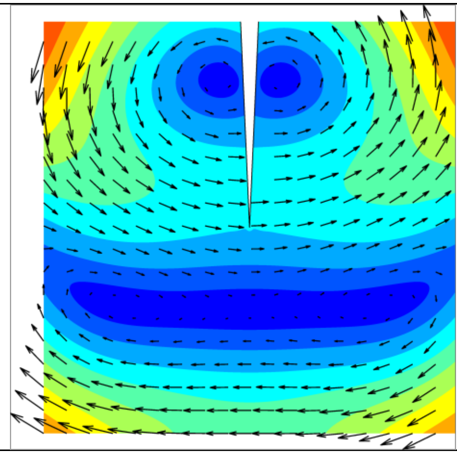
		0.316	0.796	1.180	1.212

15°	0.1	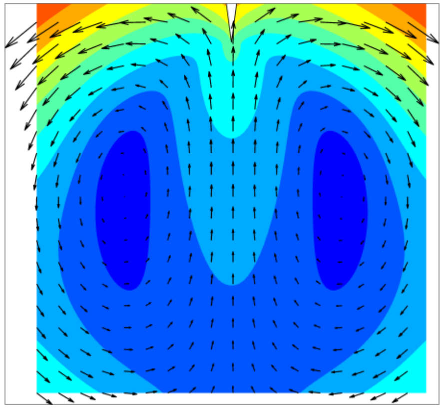	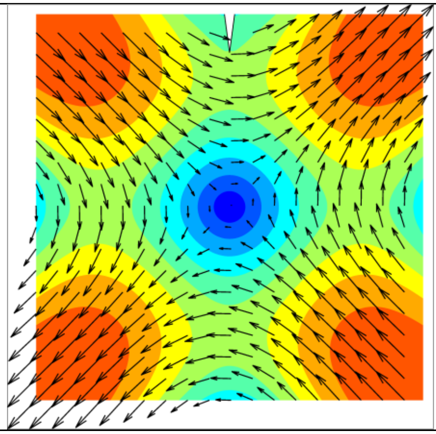	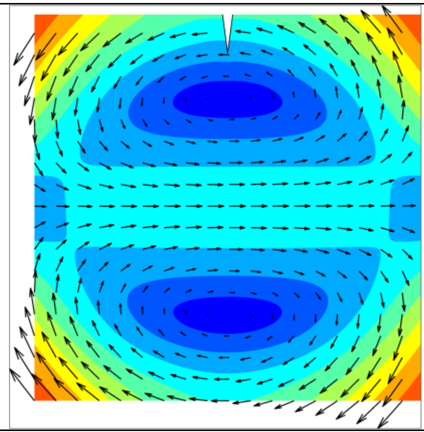	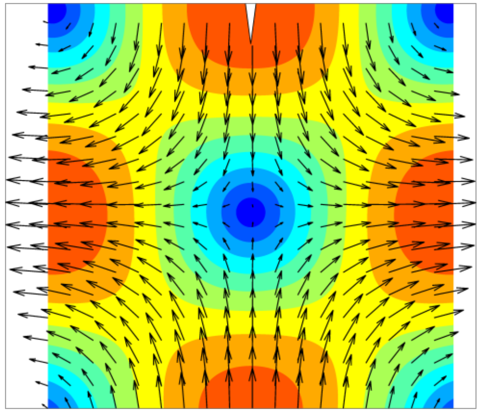
		1.083	1.160	1.236	1.316
	0.3	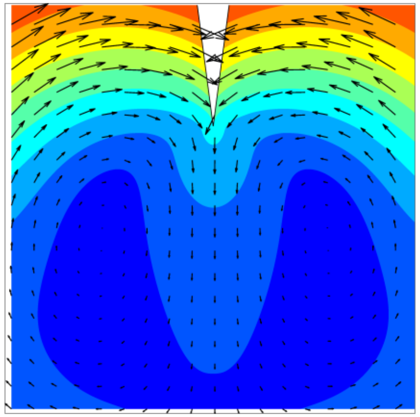	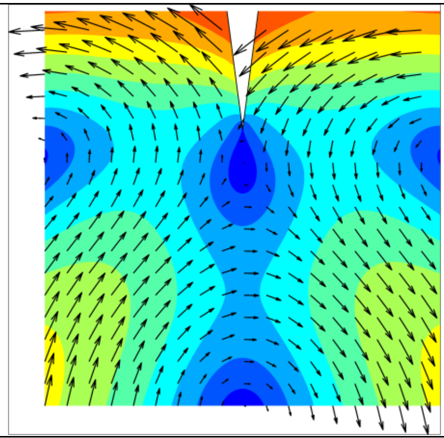	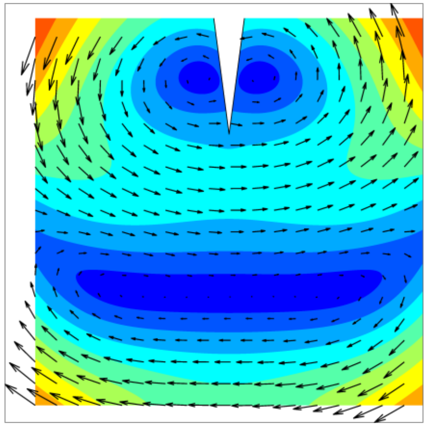	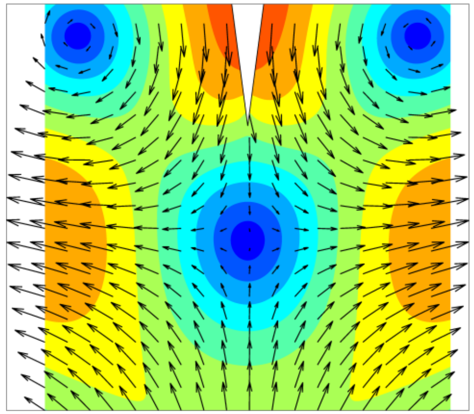
		0.580	1.078	1.215	1.311

	0.5	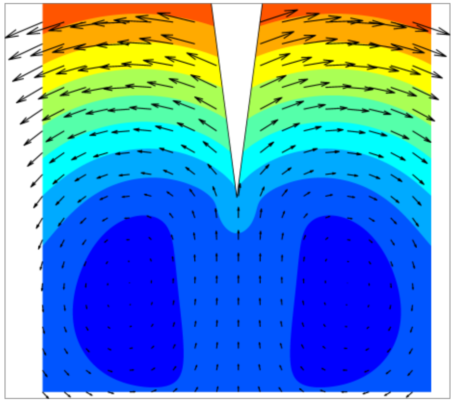	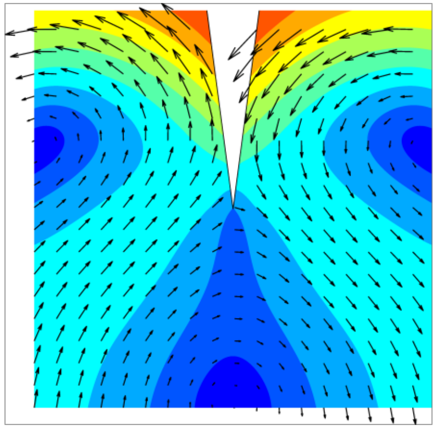	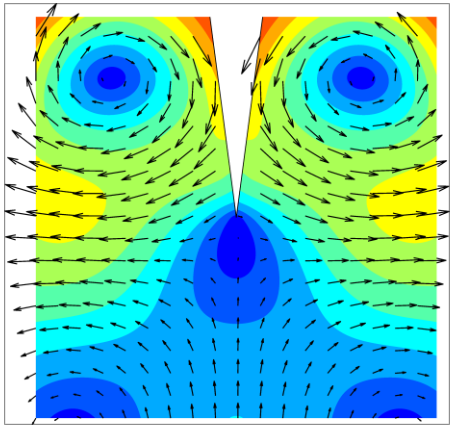	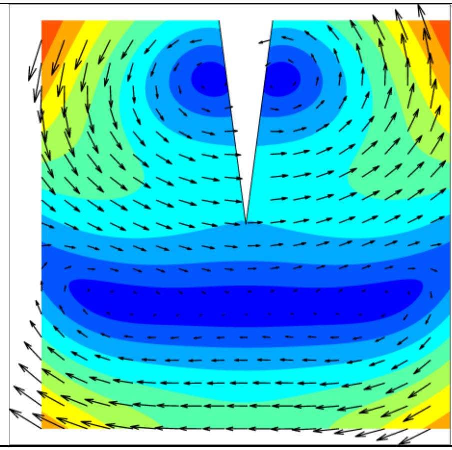
		0.325	0.797	1.191	1.214
30°	0.1	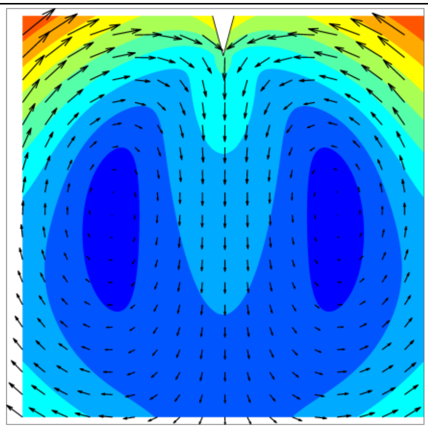	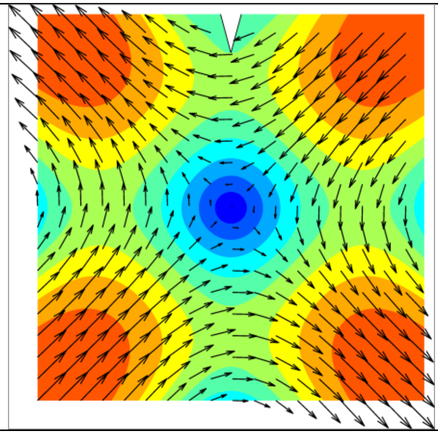	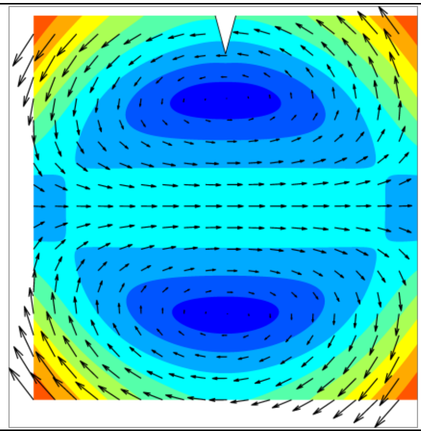	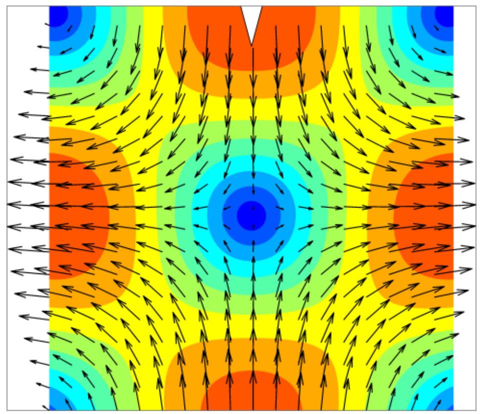
		1.086	1.160	1.236	1.317

	0.3	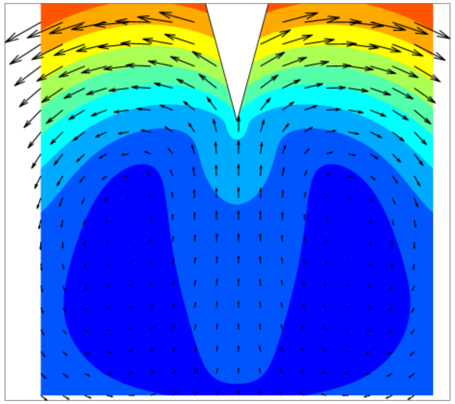	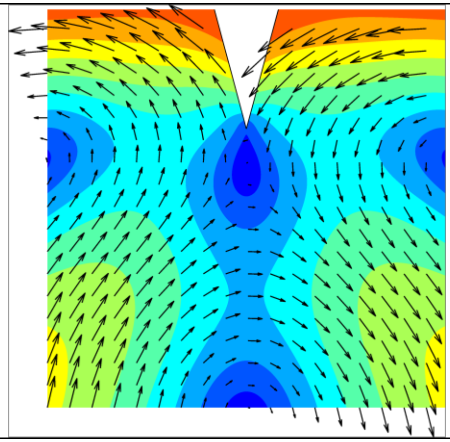	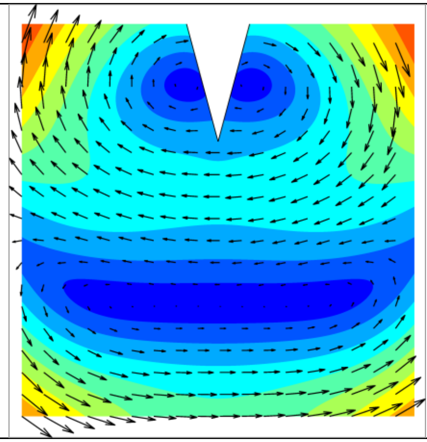	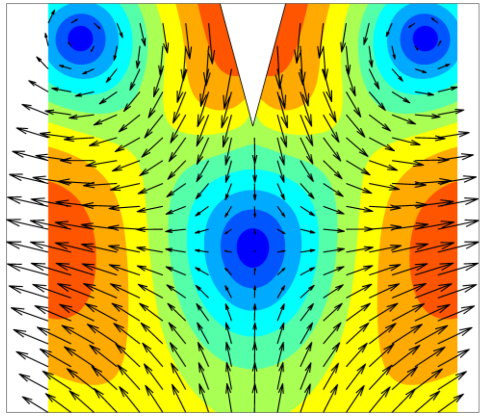
		0.595	1.082	1.216	1.325
	0.5	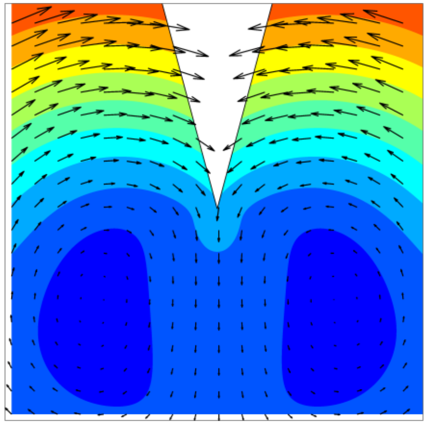	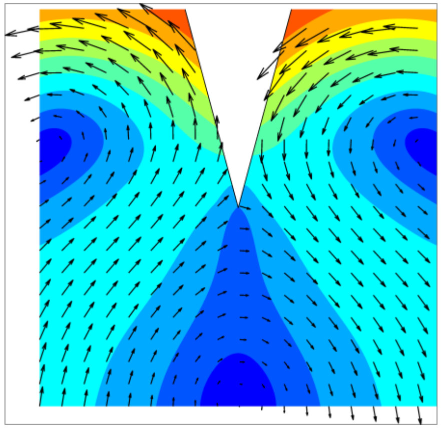	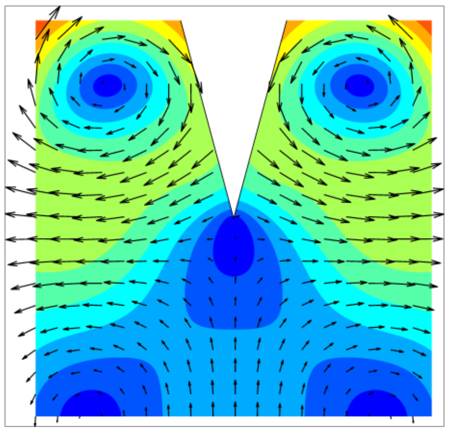	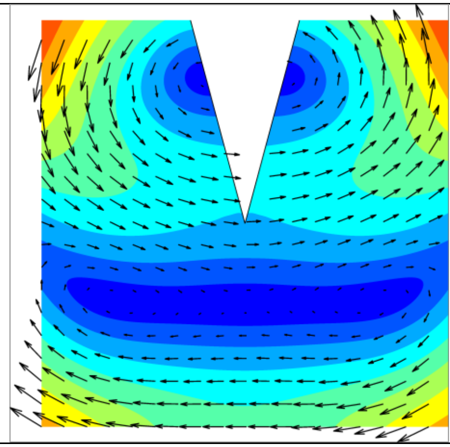
		0.342	0.810	1.204	1.218
Plot legend					

Table 8. The frequency parameters $(\omega a/2)\sqrt{\rho(1-\nu^2)/E}$ and mode shapes for a free square plate with a vertical V-notch at $c/a = 0.5$: Mode 5 to Mode 8.

Notch angle γ	d/b	Mode No. 5	6	7	8
N/A	0	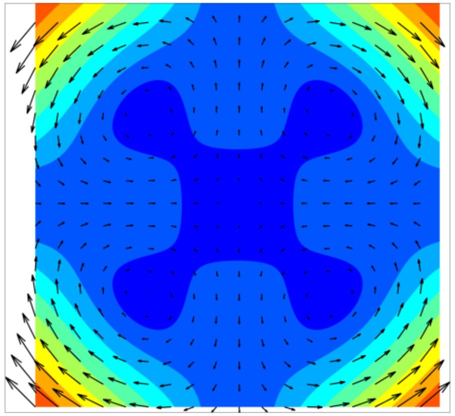	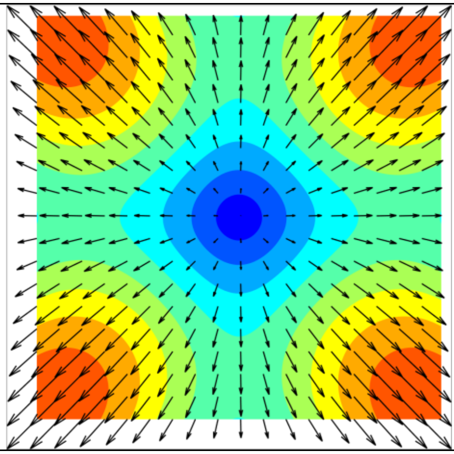	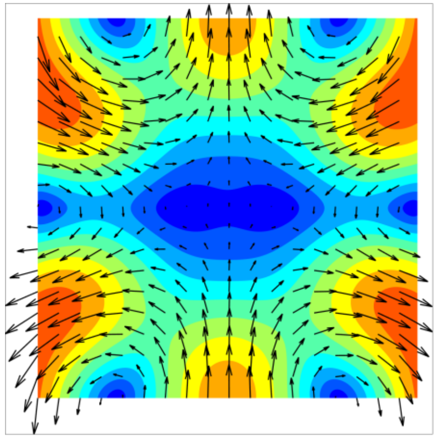	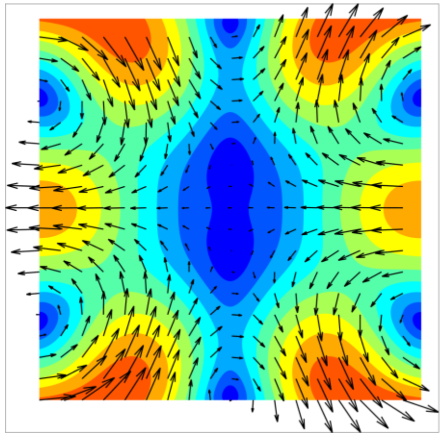
		1.494	1.726	1.862	1.862
5°	0.1	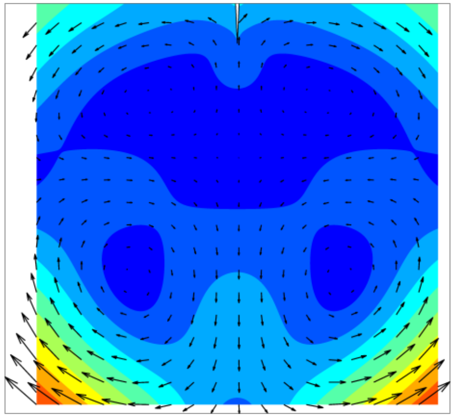	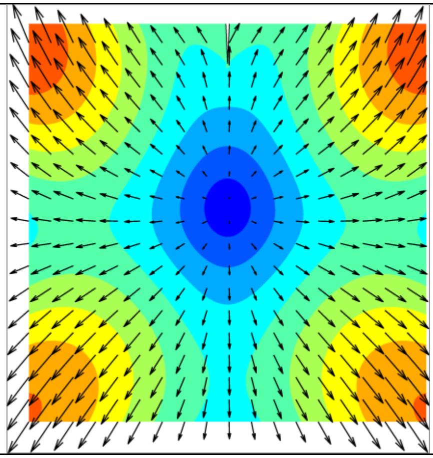	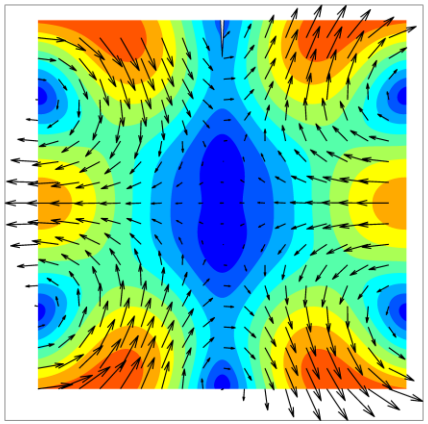	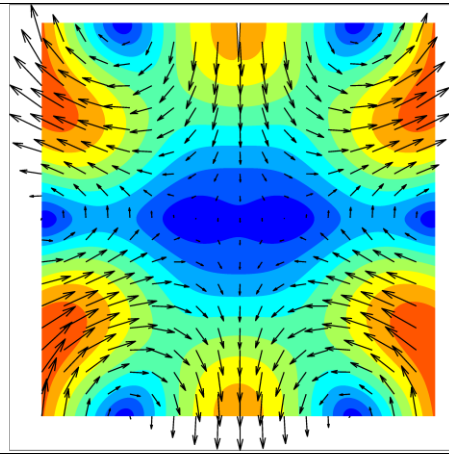
		1.427	1.709	1.858	1.862

	0.3	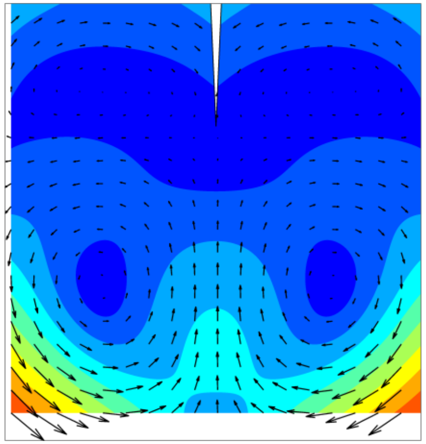	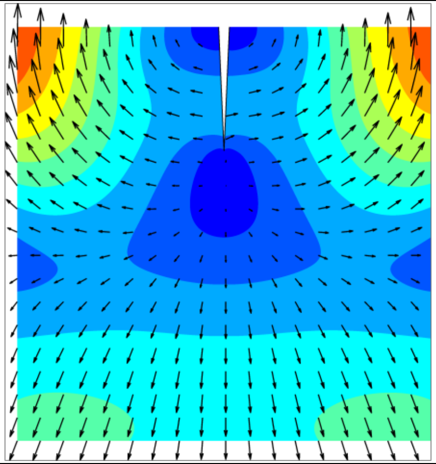	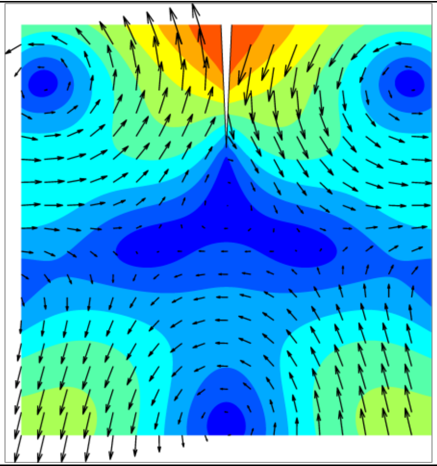	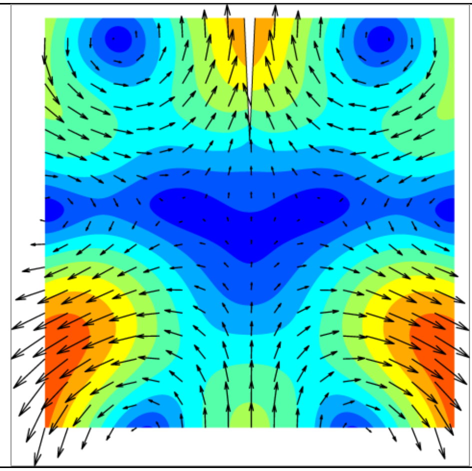
		1.400	1.635	1.653	1.839
	0.5	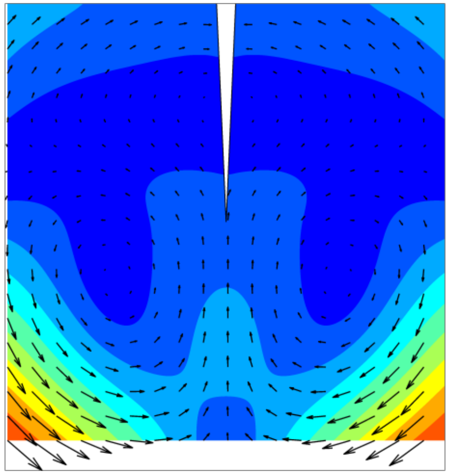	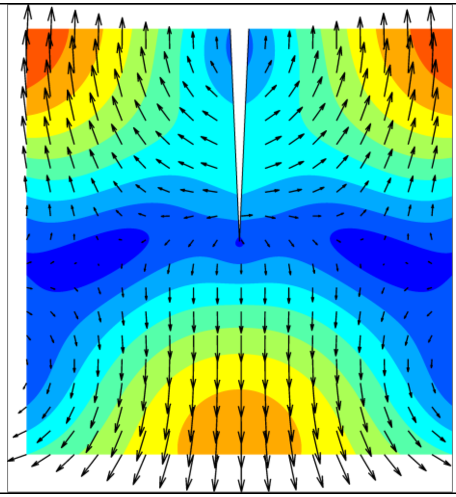	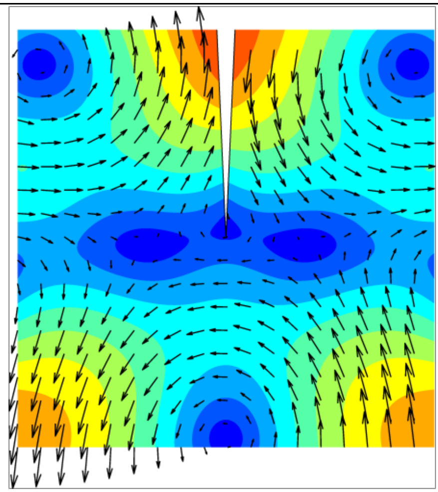	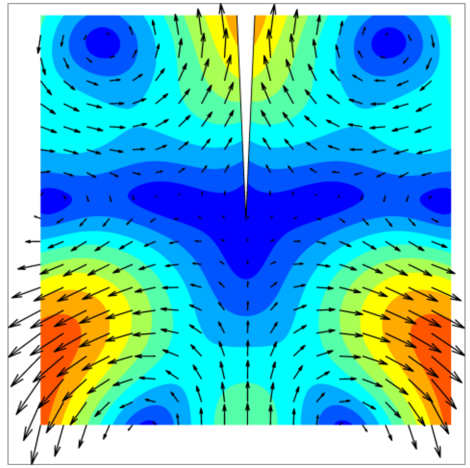
		1.388	1.527	1.556	1.832

15°	0.1	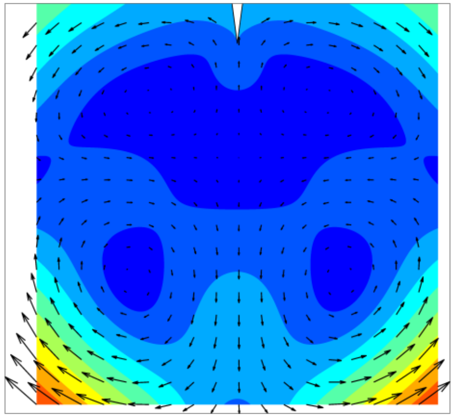	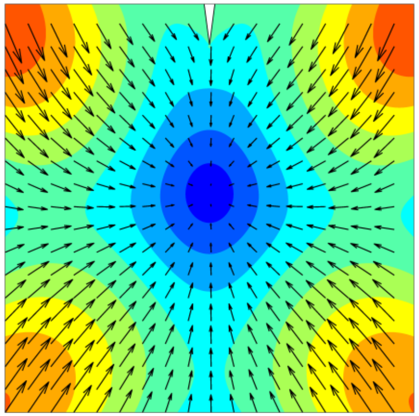	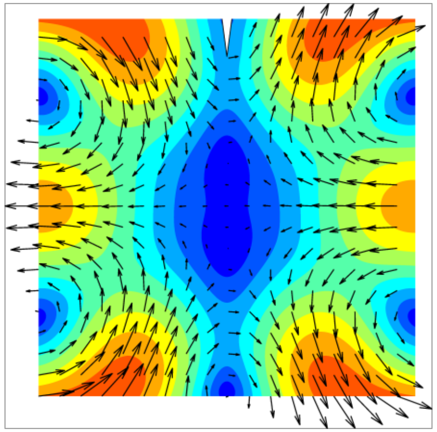	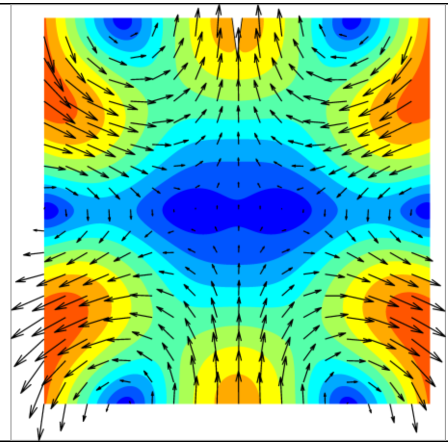
		1.428	1.709	1.858	1.863
	0.3	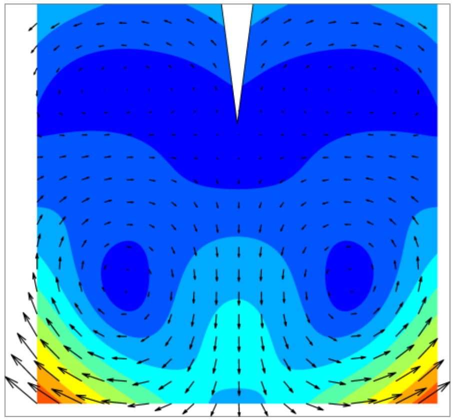	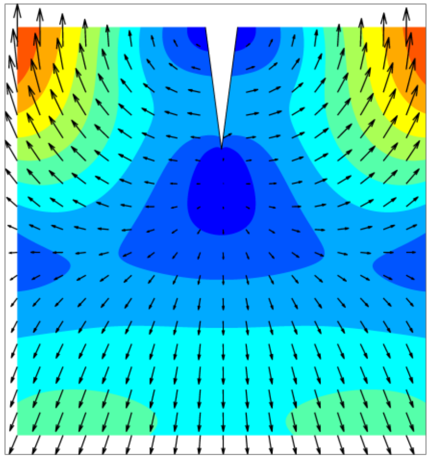	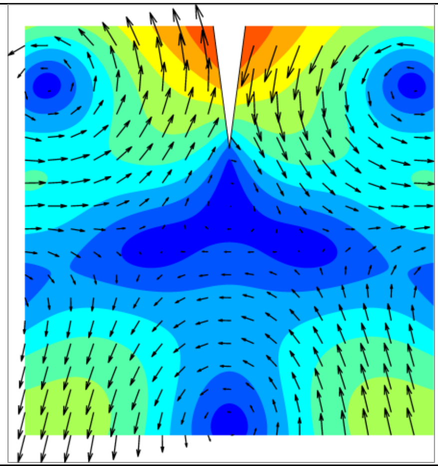	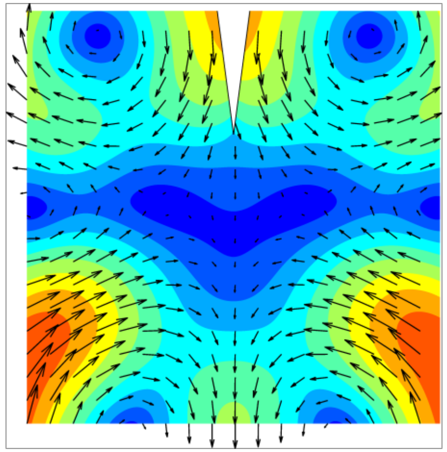
		1.402	1.635	1.657	1.852

	0.5	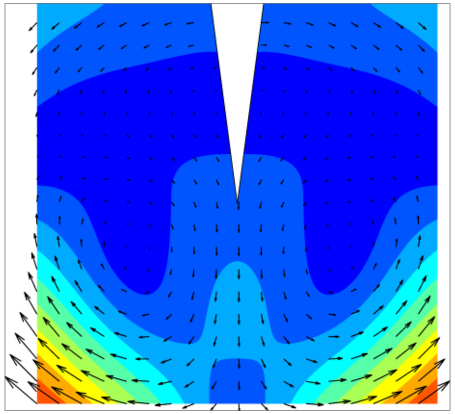	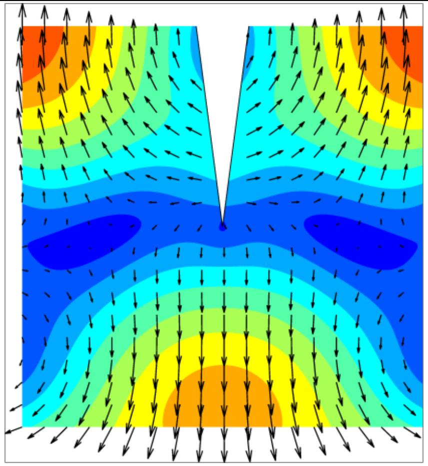	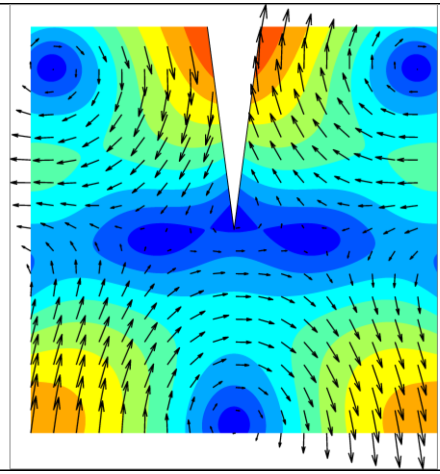	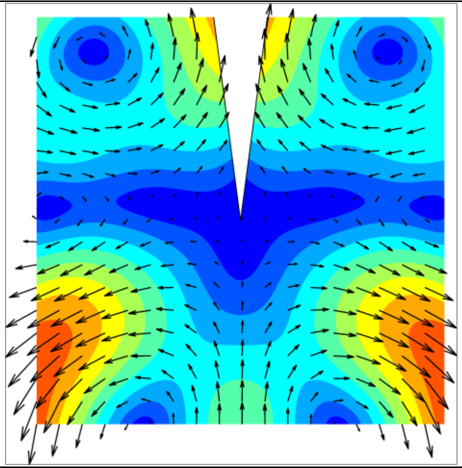
		1.388	1.533	1.580	1.851
30°	0.1	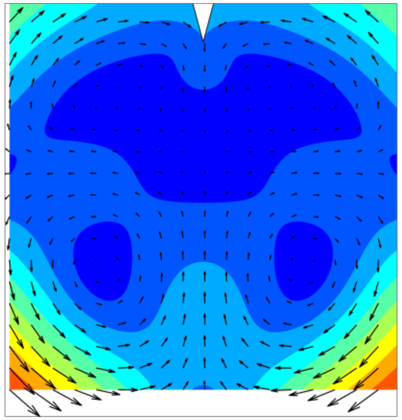	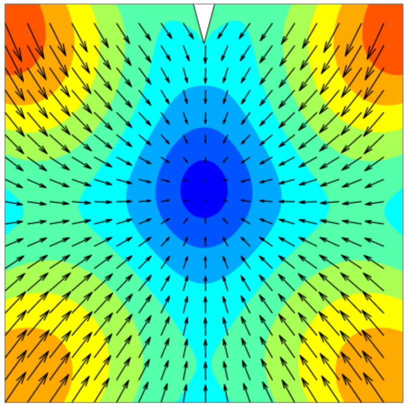	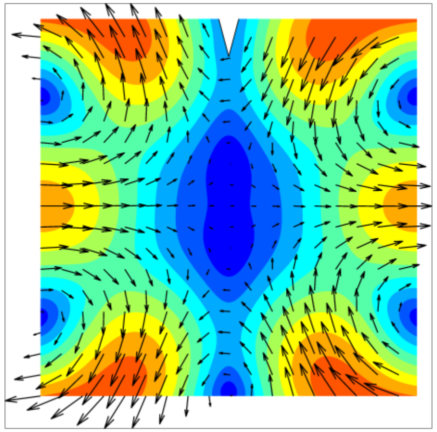	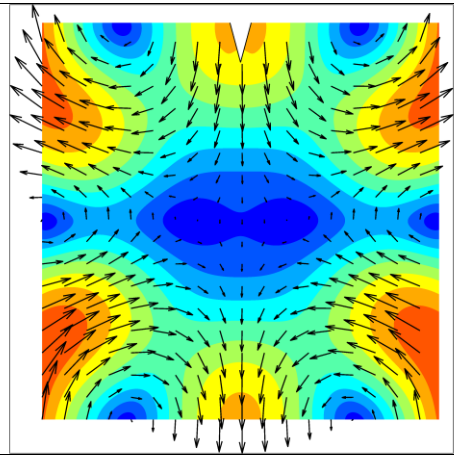
		1.429	1.710	1.858	1.866

	0.3	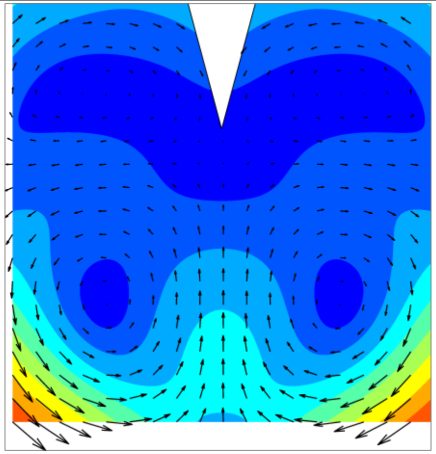	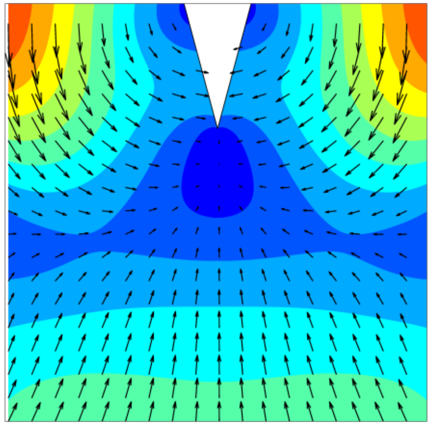	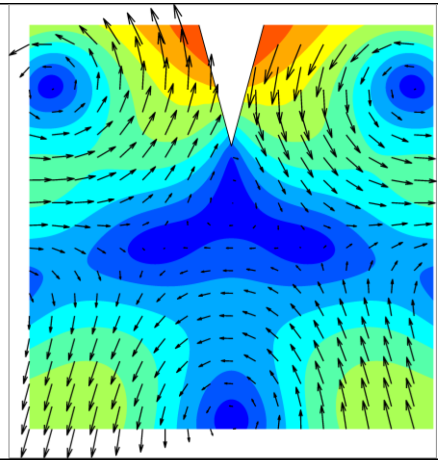	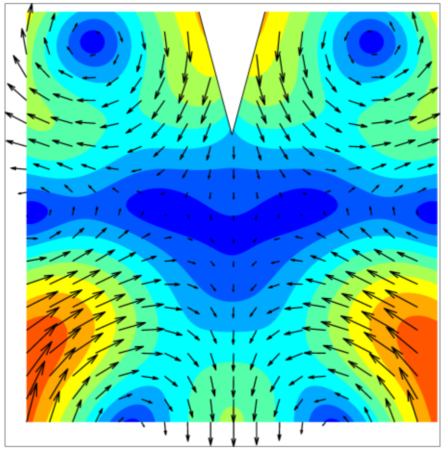
		1.404	1.637	1.671	1.870
	0.5	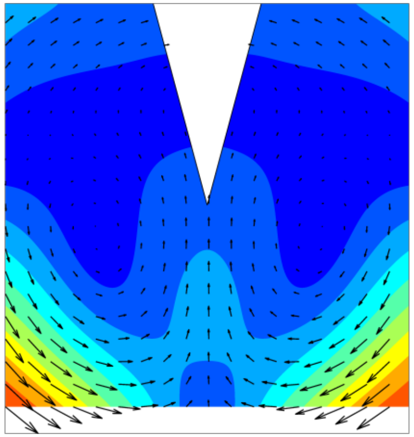	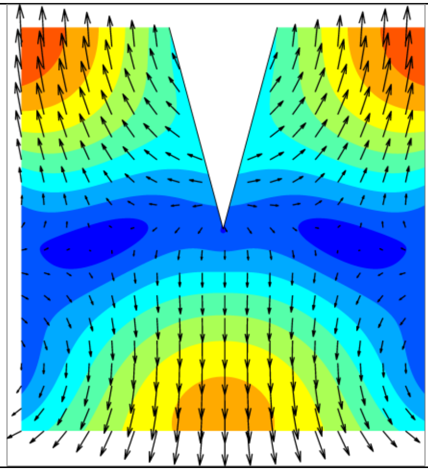	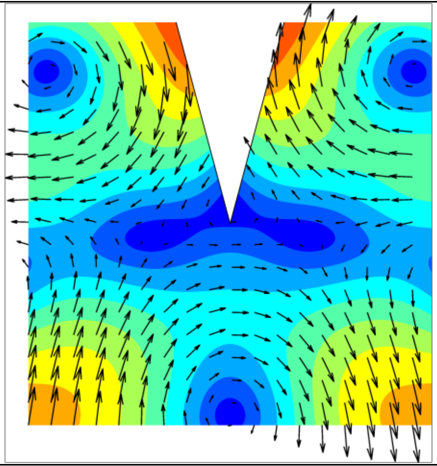	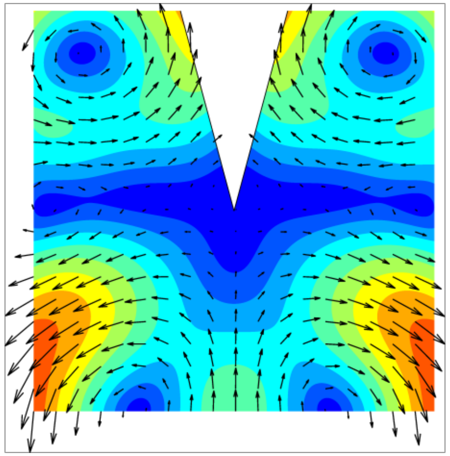
		1.387	1.543	1.614	1.876
Plot legend		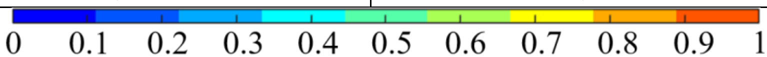			

4.1 Effects of notch depth and opening angle on the frequency parameters

After introducing the V-notch, the repeated eigenvalues split, and the ordering of the modes can change. The intact free square plate has repeated frequency parameters for modes 2 and 3, both equal to 1.236, and for modes 7 and 8, both equal to 1.862. These repeated eigenvalues arise from the rotational symmetry of the intact square plate. Introducing a centrally located V-notch preserves the symmetry about the notch but removes the rotational symmetry of the intact plate, which can change the mode ordering. This effect is already evident for the shallow notch with $d/b = 0.1$. One member of the repeated pair at 1.236 decreases to between 1.082 and 1.086, depending on the notch angle, and becomes the first mode of the notched plate. In contrast, the mode whose displacement pattern resembles the fundamental mode of the intact plate remains at approximately 1.160 and becomes the second mode. The other member of the original repeated pair is only weakly affected, remaining between 1.235 and 1.236. Thus, even though the notch is shallow, it selectively affects one orientation of the repeated modal pair and changes the sequence of the lowest frequencies.

The notch depth has a much stronger influence than the notch opening angle. When d/b increases from 0.1 to 0.3, the first frequency parameter decreases from approximately 1.08 to between 0.571 and 0.595. For the deepest notch, $d/b = 0.5$, it decreases further to between 0.316 and 0.342. These values are approximately 70% to 73% lower than the first frequency parameter of the intact plate. The corresponding mode shapes indicate that this low frequency branch is particularly sensitive to the compliance introduced by the deep notch. The second ordered frequency is also substantially reduced by increasing the notch depth, while the third, fifth, and eighth ordered frequencies are much less sensitive. Overall, the sensitivity to the notch does not decrease systematically with increasing mode number. Instead, it depends on the extent to which the modal displacement field interacts with the notch region.

The notch angle produces a secondary effect compared with the notch depth. For $d/b = 0.1$, changing γ from 5° to 30° changes each of the first eight frequency parameters by less than approximately 0.4%. The angle effect becomes more visible as the notch becomes deeper. At $d/b = 0.3$, the largest variation occurs for the first mode, whose frequency increases from 0.571 to 0.595 as the angle increases from 5° to 30°. At $d/b = 0.5$, the corresponding increase is from 0.316 to 0.342, or approximately 8% relative to the result for the 5° notch. The seventh and eighth modes also show a noticeable dependence on the notch angle for the deepest notch, whereas the fifth mode remains almost insensitive.

For most modes, increasing the notch angle at a fixed depth slightly increases the frequency parameter. This trend should not be interpreted solely in terms of stiffness loss. Widening the notch removes additional material and changes both the modal stiffness and modal mass, and the resulting frequency is governed by the ratio of these two modal quantities. A wider notch does not necessarily produce a lower frequency. For example, the eighth frequency parameter for $\gamma = 30°$ increases slightly from 1.866 at $d/b = 0.1$ to 1.876 at $d/b = 0.5$, which is slightly higher than the intact value of 1.862.

4.2 Evolution of the mode shapes

Because the notch is located at the centre of the edge, the geometry remains symmetric about its bisector. The computed mode shapes consequently exhibit either symmetric or antisymmetric behaviour with respect to this line. The notch destroys the rotational symmetry of the intact square plate, but it does not destroy the remaining mirror symmetry. This explains why repeated modes of the intact plate split while the resulting notched plate modes continue to exhibit symmetry.

For $d/b = 0.1$, most of the mode shapes remain recognisable from those of the intact plate. As the notch depth increases, the mode shapes become increasingly influenced by the two notch faces where substantial relative motion can be observed. Nevertheless, some modes retain a more consistent pattern and remain comparatively insensitive to the notch, for example the fifth and eighth modes, particularly with respect to changes in the notch angle. Overall, the effect of the V-notch is strongly mode dependent.

Huang *et al.* [26] reported that, for the transverse vibration of a free square plate, a shallow V-notch with $d/b = 0.1$ changed the first five frequencies by no more than 1.8% (with $c/a = 0.5$ and $\gamma = 30°$). In the present in-plane problem, the shallow notch reduces the first frequency by approximately 6.4% to 6.7% relative to the intact fundamental frequency and, more importantly, changes the modal ordering through the splitting of a repeated eigenvalue. The comparison indicates that the in-plane and transverse vibration fields can respond quite differently to the same local geometric discontinuity. Both studies nevertheless show that deep notches affect the natural frequencies and mode shapes substantially.

5 Conclusions

An enriched Ritz method has been developed for the free in-plane vibration of rectangular plates with an edge V-notch, combining a regular trigonometric-polynomial basis with Williams-type corner functions re-derived for the coupled in-plane displacement field. Extensive convergence studies have been presented to establish the accuracy and convergence of the method, followed by a set of benchmark results for a free square plate with a vertical V-notch. The main conclusions are as follows:

1. The proposed formulation reproduces published frequency parameters for intact rectangular plates under a range of boundary conditions, with monotonic convergence from above to at least four significant figures. For V-notched plates, where no published solutions exist, the results agree closely with finite element predictions across all configurations considered. The frequency parameters converge to at least three significant figures while preserving the upper-bound character of the Ritz method.
2. The importance of corner enrichment increases with the strength of the notch-induced singularity. For moderate notch angles ($\gamma = 90^{\circ} \sim 45^{\circ}$), where only one singular root exists per symmetry family, the improvement on accuracy over the unenriched regular basis is modest to substantial depending on singularity strength. For sharp notches ($\gamma = 15^{\circ}$ and 5°), enrichment produces large corrections. For example, a fourth-mode frequency parameter changes from 1.202 (unenriched) to 0.847 (enriched), against an ANSYS value of 0.846, which demonstrates the necessity of enrichment for accuracy. In addition, as the notch angle decreases, the regular approximation becomes increasingly inefficient for notch-sensitive modes. The corner functions supply the missing local behaviour and can substantially accelerate convergence.
3. When only one positive Williams root other than $\lambda = 1$ exists in each symmetry family, both roots should be retained. For sharper notches admitting several positive roots, the leading roots satisfying $0 < \lambda < 1$ capture the dominant local behaviour as they represent the singular stress field proportional to $r^{\lambda-1}$, while subsequently added roots with $\lambda > 1$ provide diminishing refinements. The number of corner functions required to reach converged frequencies is mode-dependent, and retaining an excessive number of corner functions may lead to ill-conditioned matrices. A practical truncation should be based on the convergence and stabilisation of frequencies, rather than including all available corner functions.
4. The effect of the V-notch is generally mode-dependent. Notch depth is the principal geometric parameter governing the frequency changes. For the cases considered, increasing d/b from 0.1 to 0.5 reduces the first ordered frequency parameter from 1.082~1.086 to 0.316~0.342, representing a reduction of approximately 70%~73% relative to the intact frequency value. The influence of notch opening angle is generally weaker than that of notch depth and becomes more evident as the notch deepens. For a shallow notch, changing the angle from 5° to 30° produces only minor changes in the first eight frequencies. For deeper notches, the angle effect becomes more pronounced for selected modes. The relationship is not uniformly monotonic because widening the notch changes both the modal stiffness and modal mass.

The enriched Ritz method presented here provides an accurate and computationally efficient tool for predicting the in-plane natural frequencies and mode shapes of V-notched rectangular plates and establishes benchmark results against which future numerical or analytical studies may be validated. Extension of the present formulation to multiple or asymmetrically located notches, laminated or orthotropic plates, and experimental validation are recommended directions for future work.

Acknowledgements

None.

Author Contributions

X. Sun: Conceptualization, Methodology, Software, Validation, Formal analysis, Investigation, Data Curation, Writing - Original Draft, Writing - Review & Editing, Visualization, Project administration.

Funding Declaration

This research did not receive any specific grant from funding agencies in the public, commercial, or not-for-profit sectors.

Statements and Declarations

The author(s) declared no potential conflicts of interest with respect to the research, authorship, and/or publication of this article.

Data Availability

The data that support the findings of this study are available from the corresponding author upon reasonable request.

References

1. Bercin AN (1996) An assessment of the effects of in-plane vibrations on the energy flow between coupled plates. J. Sound Vib. 191(5): 661-680. https://doi.org/10.1006/jsvi.1996.0149
2. Langley RS, Bercin AN (1994) Wave intensity analysis of high frequency vibrations. Philos Trans A Math Phys Eng Sci. 346(1681): 489-499. https://doi.org/10.1098/rsta.1994.0031
3. Lyon RH (1986) In-plane contribution to structural noise transmission. Noise Control Eng. J. 26(1): 22-27. https://doi.org/10.3397/1.2827659
4. Du J, Li WL, Jin G, Yang T, Liu Z (2007) An analytical method for the in-plane vibration analysis of rectangular plates with elastically restrained edges. J. Sound Vib. 306(3): 908-927. https://doi.org/10.1016/j.jsv.2007.06.011
5. Gorman DJ (2006) Exact solutions for the free in-plane vibration of rectangular plates with two opposite edges simply supported. J. Sound Vib. 294(1): 131-161. https://doi.org/10.1016/j.jsv.2005.10.023
6. Kobayashi Y, Yamada G, Honma S (1988) In-plane vibration of point-supported rectangular plates. J. Sound Vib. 126(3): 545-549. https://doi.org/10.1016/0022-460X(88)90230-1
7. Bardell NS, Langley RS, Dunsdon JM (1996) On the free in-plane vibration of isotropic rectangular plates. J. Sound Vib. 191(3): 459-467. https://doi.org/10.1006/jsvi.1996.0134
8. Wang G, Wereley NM (2002) Free in-plane vibration of rectangular plates. AIAA Journal. 40(5): 953-959. https://doi.org/10.2514/2.1732
9. Gorman DJ (2004) Accurate analytical type solutions for the free in-plane vibration of clamped and simply supported rectangular plates. J. Sound Vib. 276(1): 311-333. https://doi.org/10.1016/j.jsv.2003.07.037
10. Gorman DJ (2004) Free in-plane vibration analysis of rectangular plates by the method of superposition. J. Sound Vib. 272(3): 831-851. https://doi.org/10.1016/S0022-460X(03)00421-8
11. Liu B, Xing Y (2011) Comprehensive exact solutions for free in-plane vibrations of orthotropic rectangular plates. Eur. J. Mech. A. Solids. 30(3): 383-395. https://doi.org/10.1016/j.euromechsol.2011.01.003
12. Xing YF, Liu B (2009) Exact solutions for the free in-plane vibrations of rectangular plates. Int. J. Mech. Sci. 51(3): 246-255. https://doi.org/10.1016/j.ijmecsci.2008.12.009
13. Gutierrez RH, Laura PAA (1989) In-plane vibrations of thin, elastic, rectangular plates elastically restrained against translation along the edges. J. Sound Vib. 132(3): 512-515. https://doi.org/10.1016/0022-460X(89)90643-3
14. Dozio L (2010) Free in-plane vibration analysis of rectangular plates with arbitrary elastic boundaries. Mech. Res. Commun. 37(7): 627-635. https://doi.org/10.1016/j.mechrescom.2010.09.003
15. Dozio L (2011) In-plane free vibrations of single-layer and symmetrically laminated rectangular composite plates. Compos. Struct. 93(7): 1787-1800. https://doi.org/10.1016/j.compstruct.2011.01.021
16. Shi D, Wang Q, Shi X, Pang F (2015) A series solution for the in-plane vibration analysis of orthotropic rectangular plates with non-uniform elastic boundary constraints and internal line supports. Arch. Appl. Mech. 85(1): 51-73. https://doi.org/10.1007/s00419-014-0899-x
17. Liu T, Wang A, Wang Q, Qin B, Xie F (2021) Chebyshev formulation for in-plane vibration analysis of arbitrary laminated polygonal plates. AIAA Journal. 59(7): 2753-2767. https://doi.org/10.2514/1.J060366

18. Zhao T, Chen Y, Dai L, Linghu S, Zhang G (2023) Free in-plane vibration of irregular laminated plate with curved edges based on boundary-type chebyshev–ritz method. Thin-Walled Struct. 190: 110977. https://doi.org/10.1016/j.tws.2023.110977
19. Liu T, Wang Q, Qin B, Wang A (2022) Free in-plane vibration of plates with arbitrary curvilinear geometry: Spectral-chebyshev model and experimental study. Thin-Walled Struct. 170: 108628. https://doi.org/10.1016/j.tws.2021.108628
20. Williams M (1952) Stress singularities resulting from various boundary conditions in angular corners of plates in extension. J. Appl. Mech. 19(4): 526-528. https://doi.org/10.1115/1.4010553
21. Williams M, Surface stress singularities resulting from various boundary conditions in angular corners ofplates under bending, in The First U.S. National Congress of Applied Mechanics. 1951: Chicago, Illinois. p. 325-329.
22. Leissa AW, McGee OG, Huang CS (1993) Vibrations of circular plates having v-notches or sharp radial cracks. J. Sound Vib. 161(2): 227-239. https://doi.org/10.1006/jsvi.1993.1068
23. McGee OG, Leissa AW, Kim JW, Kim YS (2003) Vibration of plates with constrained v-notches or cracks. J. Eng. Mech. 129(7): 812-822. https://doi.org/10.1061/(ASCE)0733-9399(2003)129:7(812)
24. McGee OG, Leissa AW, Huang CS, Kim JW (1995) Vibrations of circular plates with clamped v-notches or rigidly constrained radial cracks. J. Sound Vib. 181(2): 185-201. https://doi.org/10.1006/jsvi.1995.0134
25. Kim JW, Jung HY (2004) Influence of stress singularities on the vibration of rhombic plates with v-notches or sharp cracks. Key Eng. Mater. 270-273: 1414-1419 https://doi.org/10.4028/www.scientific.net/KEM.270-273.1414
26. Huang CS, Leissa AW, Liao SC (2008) Vibration analysis of rectangular plates with edge v-notches. Int. J. Mech. Sci. 50(8): 1255-1262. https://doi.org/10.1016/j.ijmecsci.2008.05.005
27. McGee OG, Kim JW (2010) Three-dimensional vibrations of cylindrical elastic solids with v-notches and sharp radial cracks. J. Sound Vib. 329(4): 457-484. https://doi.org/10.1016/j.jsv.2009.08.011
28. Huang CH, Chen YY (2016) Investigations of the transverse vibration characteristics of piezoceramic circular plates with v-notches. J. Chin. Inst. Eng. 39(5): 593-599. https://doi.org/10.1080/02533839.2016.1146089
29. Huang CH, Chen YY (2014) Vibration analysis for piezoceramic circular plates with v-notches. Part 1: Theory. J. Mech. 30(6): 603-609. https://doi.org/10.1017/jmech.2014.53
30. Yang Y, Cheng C, Niu Z, Hu Z (2022) Free vibration analysis for v-notched mindlin plates with free or clamped radial edges. Acta Mech. 233(6): 2271-2285. https://doi.org/10.1007/s00707-022-03211-9
31. Dunavant DA (1985) High degree efficient symmetrical gaussian quadrature rules for the triangle. Int. J. Numer. Methods Eng. 21(6): 1129-1148. https://doi.org/10.1002/nme.1620210612
32. Gorman DJ (2005) Free in-plane vibration analysis of rectangular plates with elastic support normal to the boundaries. J. Sound Vib. 285(4): 941-966. https://doi.org/10.1016/j.jsv.2004.09.017